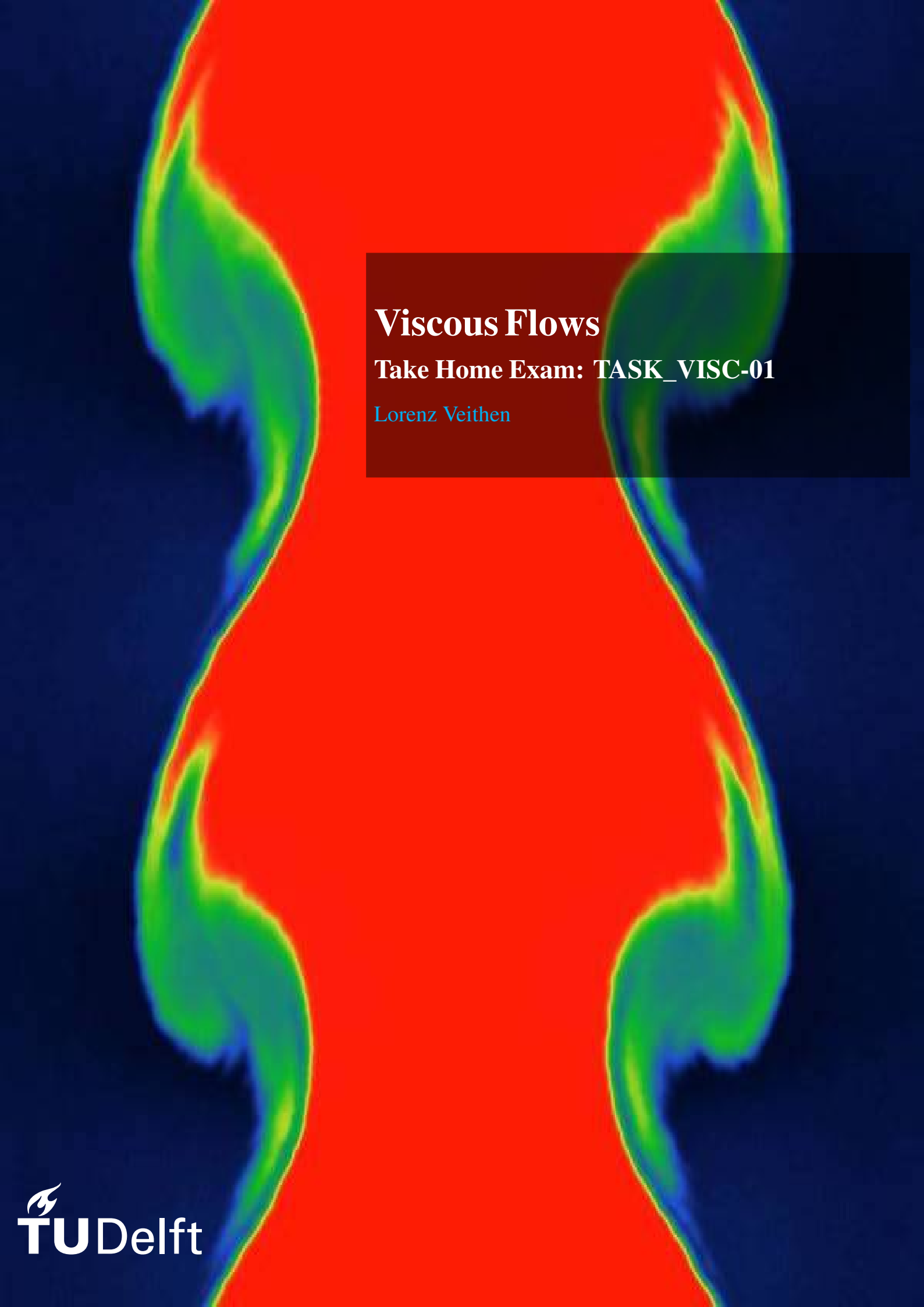

Viscous Flows

Take Home Exam: TASK_VISC-01

Lorenz Veithen

TU Delft

DELFT UNIVERSITY OF TECHNOLOGY

FACULTY OF AEROSPACE ENGINEERING

AE4120

VISCOUS FLOWS

Viscous Flows Take-Home Exam: TASK_VISC-01

Lecturers: B. van Oudheusden and M. Kotsonis

February 21, 2023

Lorenz Veithen 5075211

[1]Front Image by: Daniel Price/science Photo Library https://fineartamerica.com/profiles/science-photo-library

Contents

Problem 1.E – Deformation and Vorticity 1

In this problem, two two-dimensional incompressible flow fields are analysed. The velocity in the x-direction is called u and the velocity in the y-direction is called v, the two flow fields are given by Equations (1.1) and (1.2). Note that x and y refer to the Cartesian coordinate system.

$$\vec{V_1} = \begin{bmatrix} Ax \\ -Ay \end{bmatrix} \tag{1.1}$$

$$\vec{V_2} = \begin{bmatrix} Ay \\ Ax \end{bmatrix} \tag{1.2}$$

1.1 Irrational, Continuity, and Streamlines

Introducing the methods which will be used in this section, the following points are noted:

1. A flow is **irrotational** if $curl\ \vec{V} = \nabla \times \vec{V} = \vec{0}$. That is, if the flow vorticity is zero.
2. The **incompressible continuity** equation is given by $\nabla \cdot \vec{V} = 0$. The flow divergence is zero.
3. The shape of the **streamlines** in a 2D flow is obtained by considering the differential equation $\frac{dy}{dx} = \frac{v}{u}$.

Note that for generality, the computations below are performed in their three-dimensional formulation, by putting the third velocity component of each velocity field to zero.

1.1.1 Flow 1

The flow is irrotational, computing the curl of the velocity profile, the following is found,

$$\begin{aligned} \nabla \times \vec{V_1} &= \begin{vmatrix} \hat{i} & \hat{j} & \hat{k} \\ \frac{\partial}{\partial x} & \frac{\partial}{\partial y} & \frac{\partial}{\partial z} \\ Ax & -Ay & 0 \end{vmatrix} \\ &= \left(\frac{\partial(0)}{\partial y} - \frac{\partial(-Ay)}{\partial z} \right) \hat{i} - \left(\frac{\partial(0)}{\partial x} - \frac{\partial(Ax)}{\partial z} \right) \hat{j} + \left(\frac{\partial(-Ay)}{\partial x} - \frac{\partial(Ax)}{\partial y} \right) \hat{k} \\ &= \vec{0} \end{aligned} \tag{1.3}$$

which proves that the flow is irrotational. Furthermore, the flow satisfies the incompressible continuity equation, as seen from the following,

$$\nabla \cdot \vec{V_1} = \frac{\partial(Ax)}{\partial x} + \frac{\partial(-Ay)}{\partial y} + \frac{\partial(0)}{\partial z} = A - A + 0 = 0 \tag{1.4}$$

which proves that the flow satisfies the incompressible continuity equation. The shape of the streamlines is obtained by considering the following ordinary differential equation,

$$\begin{aligned} \frac{dy}{dx} = \frac{v}{u} &= \frac{-Ay}{Ax} \\ \Leftrightarrow \frac{dy}{y} &= \frac{-dx}{x} \\ \Leftrightarrow \ln y &= -\ln x + C_1 \\ \Leftrightarrow \ln y &= \ln x^{-1} + \ln C_2 \\ \Leftrightarrow y &= \frac{C_2}{x} \end{aligned} \tag{1.5}$$

The direction of the flow lines is obtained by considering the velocity vector in each quadrant of the coordinate system. In the first quadrant, both the x and y coordinates are positive, meaning that the first component of the velocity field points towards the positive x and the second component points towards the negative y. This results in a flow going 'down and to the right' on the streamlines described by $y = \frac{C_2}{x}$. The opposite is true for the third quadrant. In the second quadrant, the x coordinate is negative but the y is positive, therefore, the first component of the velocity vectors points towards the negative x and the second towards the negative y. This results in a flow going 'down and to the left' on the streamlines. The opposite is true for the fourth quadrant. It is additionally noted that the flow clearly shows two asymptotes which are the axis of the coordinate system: the fluid flow comes from the $x = 0$ (y-axis) asymptote and goes towards the $y = 0$ (x-axis) asymptote. The streamlines are shown in Figure 1.1.

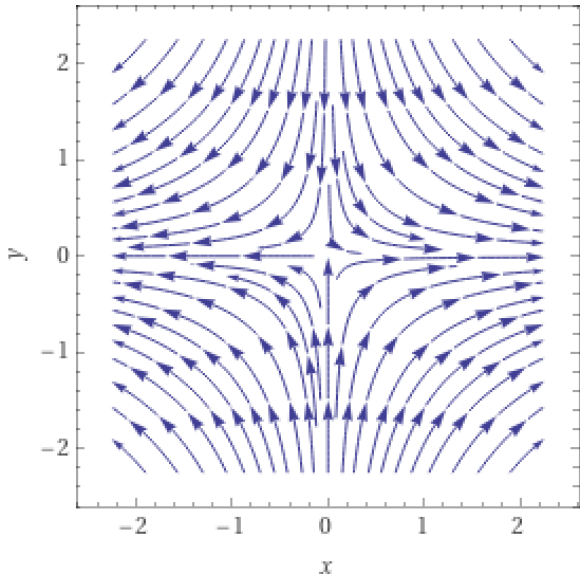

Figure 1.1: Flow pattern of the flow described by the V_1 velocity field. This plot was generated using WolframAlpha.

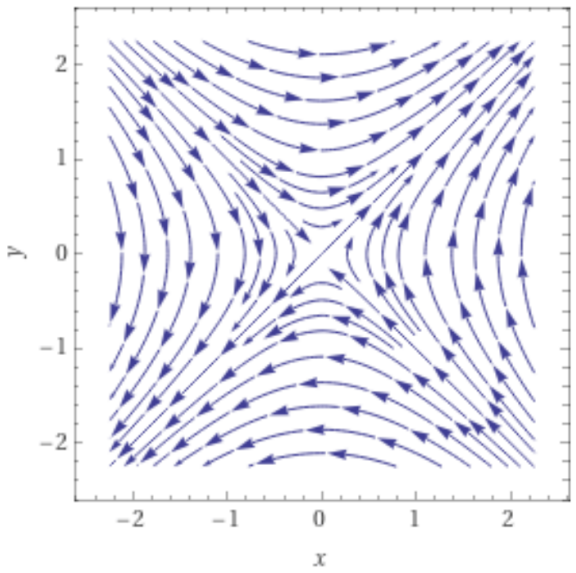

Figure 1.2: Flow pattern of the flow described by the V_2 velocity field. This plot was generated using WolframAlpha.

1.1.2 Flow 2

The same steps can be applied to the second velocity field. Starting with the irrationality assessment,

$$\begin{aligned}\nabla \times \vec{V_2} &= \begin{vmatrix} \hat{i} & \hat{j} & \hat{k} \\ \frac{\partial}{\partial x} & \frac{\partial}{\partial y} & \frac{\partial}{\partial z} \\ Ay & Ax & 0 \end{vmatrix} \\ &= \left(\frac{\partial(0)}{\partial y} - \frac{\partial(Ax)}{\partial z}\right)\hat{i} - \left(\frac{\partial(0)}{\partial x} - \frac{\partial(Ay)}{\partial z}\right)\hat{j} + \left(\frac{\partial(Ax)}{\partial x} - \frac{\partial(Ay)}{\partial y}\right)\hat{k} \\ &= 0\hat{i} - 0\hat{j} + (A - A)\hat{k} = \vec{0} \end{aligned} \tag{1.6}$$

which proves that the flow is irrotational. Considering the incompressible continuity equation,

$$\nabla \cdot \vec{V_2} = \frac{\partial(Ay)}{\partial x} + \frac{\partial(Ax)}{\partial y} + \frac{\partial(0)}{\partial z} = 0 \tag{1.7}$$

which proves that the flow field satisfies the incompressible continuity equation. The shape of the streamlines is then obtained by considering the following ordinary differential equation,

$$\begin{aligned}\frac{dy}{dx} &= \frac{v}{u} = \frac{Ax}{Ay} \\ &\Leftrightarrow ydy = xdx\end{aligned}$$

$$\Leftrightarrow \frac{y^2}{2} = \frac{x^2}{2} + D$$
$$\Leftrightarrow y = \pm\sqrt{x^2 + K} \tag{1.8}$$

It is clear that the flow pattern has two asymptotes in the far field: $y = x$ and $y = -x$. The particles come from the $y = -x$ asymptote and go towards the $y = x$ asymptote (from both directions), as time progresses. Similarly to the case of the first velocity flow field, the direction of the particles on the streamlines can be determined by considering the four quadrants independently. In the first quadrant, both x and y are positive, meaning that both components of the velocity profile are positive. Therefore, the particles progress to the right and upwards along the streamlines in that quadrant. The exact opposite applies to the third quadrant, where both x and y are negative. In the second quadrant, x is negative while y is positive: the first velocity component (u) is positive while the second is negative. Therefore, the flow progresses to the right and downwards overall on the streamlines. Again, the opposite is true in the fourth quadrant. Note that each quadrant is divided in two by one of the two asymptotes. Particles seem to originate from the $y = -x$ asymptote, present in the second and fourth quadrants and go towards the $y = x$ one present in the first and third quadrants. Note additionally, the flow lines are tangent to the horizontal (quadrant junctions IV-I and II-III) and to the vertical (quadrant junctions II-I and IV-III) at the boundaries between quadrants, linking the general directions described above. The streamline pattern is given by Figure 1.2.

1.2 Fluid Element Transport and Deformation

Taking an initial position and a square shape of a fluid element at a time t_0, the overall shape and position of the same element can be considered at a time t_1 occurring Δt seconds later. For both velocity fields being considered, the transportation of a given fluid element occurs along a streamline (in the direction indicated), as depicted in Figures 1.1 and 1.2. To obtain the position of the fluid cell after a given Δt from an initial position, the following differential equation are to be solved,

$$\begin{cases} \frac{dx}{dt} &= u \\ \frac{dy}{dt} &= v \end{cases}$$

this results in the change in x and y as a function of time, from the initial position. Following, the deformation of the fluid element is given by the strain rate tensor from Equation (1.9),

$$\epsilon_{ij} = \frac{1}{2}\left(\frac{\partial u_i}{\partial x_j} + \frac{\partial u_j}{\partial x_i}\right) = \begin{pmatrix} \epsilon_{xx} & \epsilon_{xy} \\ \epsilon_{yx} & \epsilon_{yy} \end{pmatrix} \tag{1.9}$$

With,

$$\epsilon_{xx} = \frac{\partial u}{\partial x} \qquad \epsilon_{xy} = \epsilon_{yx} = \frac{1}{2}\left(\frac{\partial u}{\partial y} + \frac{\partial v}{\partial x}\right) \qquad \epsilon_{yy} = \frac{\partial v}{\partial y}$$

Note that the diagonal terms of the strain rate tensor indicate extensional strain rates of the fluid element, while the off-diagonal elements indicate shearing strain rates. Following, the stresses on the fluid element are given by Equation (1.10) (note that the second step of the derivation is performed as both flows satisfy the incompressible continuity equation),

$$\begin{aligned} \sigma_{ij} &= -p\delta_{ij} + \tau_{ij}(\epsilon_{ij}) \\ &= -p\delta_{ij} + \mu\left(\frac{\partial u_i}{\partial x_j} + \frac{\partial u_j}{\partial x_i}\right) + \lambda\delta_{ij}(\nabla \cdot \vec{V}) \\ &= -p\delta_{ij} + \mu\left(\frac{\partial u_i}{\partial x_j} + \frac{\partial u_j}{\partial x_i}\right) \\ &= -p\delta_{ij} + 2\mu\epsilon_{ij} \end{aligned} \tag{1.10}$$

Also note that the latter holds for a Newtonian isotropic fluid. Those developments permit to analyse the two flow fields mentioned earlier.

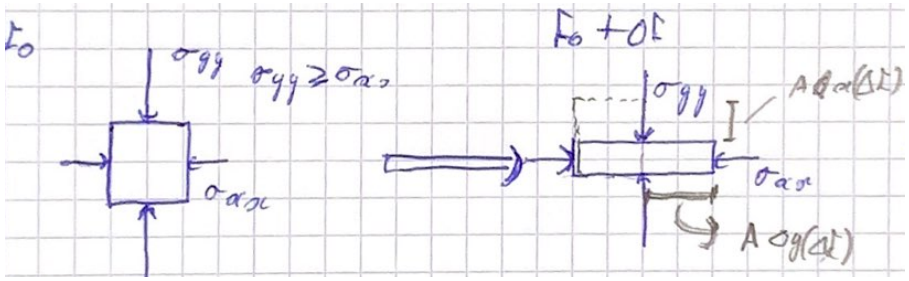

Figure 1.3: Deformation and stresses acting on a fluid element in the fluid flow 1. Note that the volume stays constant during the deformation.

1.2.1 Flow 1

The transport of the fluid element generally occurs towards the asymptotes of the flow. Solving the ordinary differential equations mentioned above,

$$\begin{aligned} \frac{dx}{dt} &= Ax \\ \Leftrightarrow \frac{dx}{x} &= Adt \\ \Leftrightarrow \ln x &= A(t-t_0) + \ln x_0 \\ \Leftrightarrow x &= x_0 e^{A\Delta t} \end{aligned} \tag{1.11}$$

$$\begin{aligned} \frac{dy}{dt} &= -Ay \\ \Leftrightarrow \frac{dy}{y} &= -Adt \\ \Leftrightarrow \ln y &= -A(t-t_0) + \ln y_0 \\ \Leftrightarrow y &= y_0 e^{-A\Delta t} \end{aligned} \tag{1.12}$$

This result is in direct agreement with the observations made from Figure 1.1. The deformation of the fluid element, as described by Equation (1.9) is then given as,

$$\begin{pmatrix} \epsilon_{xx} & \epsilon_{xy} \\ \epsilon_{yx} & \epsilon_{yy} \end{pmatrix} = \begin{pmatrix} \frac{\partial(Ax)}{\partial x} & \frac{1}{2}\left(\frac{\partial(Ax)}{\partial y} + \frac{\partial(-Ay)}{\partial x}\right) \\ \frac{1}{2}\left(\frac{\partial(-Ay)}{\partial x} + \frac{\partial(Ax)}{\partial y}\right) & \frac{\partial(-Ay)}{\partial y} \end{pmatrix} = \begin{pmatrix} A & 0 \\ 0 & -A \end{pmatrix} \tag{1.13}$$

which shows that the fluid element only experiences extensional strain rates. However, the volume of the element does not change, as was seen from the incompressible continuity equation: no mass is either created or destroyed within the fluid element. This explains why the two extensional strain rates complete each other out: when one dimension extends, the other shrinks.
Following, the stress tensor of the fluid flow is obtained from (1.10),

$$\sigma_{ij} = \begin{pmatrix} -p + 2\mu\epsilon_{xx} & 2\mu\epsilon_{xy} \\ 2\mu\epsilon_{yx} & -p + 2\mu\epsilon_{yy} \end{pmatrix} = \begin{pmatrix} -p + 2\mu A & 0 \\ 0 & -p - 2\mu A \end{pmatrix} \tag{1.14}$$

It is clear that a larger stress is applied on the y face in the y-direction ($A \geq 0$), where the strain rate is negative. Furthermore, focusing on the viscous stresses (not considering the pressure component) it is clear that only normal stresses occur on the element. This is consistent with the observation that no shear strain rates are experienced by the element in the flow. Figure 1.3 shows the deformation of the fluid element after a time Δt from the initial conditions. Figure 1.1 already showed the transport of the fluid element in the coordinate system, as time progresses.

1.2.2 Flow 2

Similarly, the second flow can be analysed in the same terms. Starting with the transport of the fluid cell in the flow field, the flow field describes a system of first order differential equations, which can be solved as follows. Setting up the system of differential equations,

$$\begin{bmatrix} \frac{dx}{dt} \\ \frac{dy}{dt} \end{bmatrix} = \begin{bmatrix} 0 & A \\ A & 0 \end{bmatrix} \begin{bmatrix} x \\ y \end{bmatrix} = B\vec{r}$$

where B is a matrix. To solve those equations, the system needs to be diagonalised. First, the eigenvalues of B are determined by solving,

$$\det(B-\lambda I)=\begin{vmatrix}-\lambda & A\\ A & -\lambda\end{vmatrix}=\lambda^2-A^2=0$$

This yields $\lambda_{1,2}=\pm A$. Then, the eigenvector associated to each eigenvalue is determined by solving $(B-\lambda I)\vec{v}=\vec{0}$. For the first eigenvalue ($\lambda=A$),

$$\begin{bmatrix}-A & A\\ A & -A\end{bmatrix}\begin{bmatrix}v_1\\ v_2\end{bmatrix}=\vec{0}$$

which yields: $v_1=v_2$ (note that both equations are essentially the same, as expected). This gives the first eigenvector $\vec{v_a}=[1\quad 1]^T$. Similarly, the second eigenvector is found to be $\vec{v_b}=[-1\quad 1]^T$ based on the second eigenvalue. This permits to formulate the two matrices (note that $C^{-1}BC=\Lambda$),

$$\Lambda=\begin{bmatrix}A & 0\\ 0 & -A\end{bmatrix}\qquad\qquad C=[\vec{v_a}\quad\vec{v_b}]=\begin{bmatrix}1 & -1\\ 1 & 1\end{bmatrix}$$

Defining a vector $\vec{z}$ such that, $\vec{r}=C\vec{z}$, the system can be diagonalised as: $\frac{d\vec{z}}{dt}=\Lambda\vec{z}$. This then gives two decoupled ordinary differential equations which can be solved straightforwardly,

$$\begin{cases}\frac{dz_1}{dt} & =Az_1\Leftrightarrow z_1(t)=K_1e^{At}\\ \frac{dz_2}{dt} & =-Az_2\Leftrightarrow z_2(t)=K_2e^{-At}\end{cases}$$

Which yields the solution in the original x-y coordinates,

$$\vec{r}=\begin{bmatrix}x(t)\\ y(t)\end{bmatrix}=C\vec{z}\Rightarrow\begin{cases}x(t)=K_1e^{At}-K_2e^{-At}\\ y(t)=K_1e^{At}+K_2e^{-At}\end{cases}$$

Linking the integration constants to the initial position x_0, y_0 and the time interval Δt, the integration constants are found to be: $K_1=\frac{x_0+y_0}{2}e^{-At_0}$ and $K_2=\frac{y_0-x_0}{2}e^{At_0}$. The fluid element is then transported according to,

$$\begin{cases}x(t)=\frac{x_0+y_0}{2}e^{A\Delta t}-\frac{y_0-x_0}{2}e^{-A\Delta t}\\ y(t)=\frac{x_0+y_0}{2}e^{A\Delta t}+\frac{y_0-x_0}{2}e^{-A\Delta t}\end{cases}\tag{1.15}$$

This result is consistent with the flow pattern shown in Figure 1.2. The deformation of the fluid element can be obtained using Equation (1.9).

$$\begin{pmatrix}\epsilon_{xx} & \epsilon_{xy}\\ \epsilon_{yx} & \epsilon_{yy}\end{pmatrix}=\begin{pmatrix}\frac{\partial(Ay)}{\partial x} & \frac{1}{2}\left(\frac{\partial(Ay)}{\partial y}+\frac{\partial(Ax)}{\partial x}\right)\\ \frac{1}{2}\left(\frac{\partial(Ax)}{\partial x}+\frac{\partial(Ay)}{\partial y}\right) & \frac{\partial(Ax)}{\partial y}\end{pmatrix}=\begin{pmatrix}0 & A\\ A & 0\end{pmatrix}\tag{1.16}$$

As only the off-diagonal terms are non-zero, this indicates that the fluid element only encounters shear strain rates in the flow field. Note again that the volume of the fluid element does not change (no creation or destruction of material in the volume). Following, the stresses on the fluid element can be assessed using Equation (1.10). The result is consistent with the observations made based on the strain rate (obviously): the fluid element is only subject to viscous shear stresses and to normal pressure stresses. Furthermore, in this case, all the viscous stresses have the same magnitude.

$$\sigma_{ij}=\begin{pmatrix}-p+2\mu\epsilon_{xx} & 2\mu\epsilon_{xy}\\ 2\mu\epsilon_{yx} & -p+2\mu\epsilon_{yy}\end{pmatrix}=\begin{pmatrix}-p & 2\mu A\\ 2\mu A & -p\end{pmatrix}\tag{1.17}$$

Figure 1.4 shows the deformation of the fluid element after a time Δt from the initial conditions. Figure 1.2 already showed the transport of the fluid element in the coordinate system, as time progresses.

1.3 Effect of Element Orientation on Stresses

Considering the flow patterns shown in Figures 1.1 and 1.2, it becomes obvious that both flow fields are effectively the same. Indeed, rotating the second flow field by an angle θ (seems to be about -45°) results in the first one, as shown below. If the second flow field is indeed only a rotation of the first one by an angle θ, V_1 can be written as a function of V_2 as,

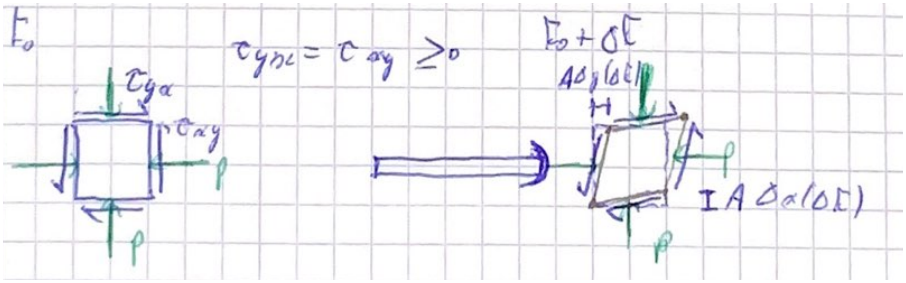

Figure 1.4: Deformation and stresses acting on a fluid element in the fluid flow 2. Note that the volume stays constant during the deformation.

$$V_1 = T_{12} V_2 = T_{12} A \begin{bmatrix} y_2 \\ x_2 \end{bmatrix}$$

Where the rotation matrix T_{12} is given by Equation (1.18),

$$T_{12} = \begin{bmatrix} \cos\theta & -\sin\theta \\ \sin\theta & \cos\theta \end{bmatrix} \tag{1.18}$$

Furthermore, this implies that the (x_2, y_2) coordinates can be expressed in terms of the (x_1, y_1) ones from,

$$\begin{bmatrix} x_1 \\ y_1 \end{bmatrix} = T_{12} \begin{bmatrix} x_2 \\ y_2 \end{bmatrix} \Leftrightarrow \begin{bmatrix} x_2 \\ y_2 \end{bmatrix} = T_{12}^{-1} \begin{bmatrix} x_1 \\ y_1 \end{bmatrix} = \begin{bmatrix} \cos\theta & \sin\theta \\ -\sin\theta & \cos\theta \end{bmatrix} \begin{bmatrix} x_1 \\ y_1 \end{bmatrix}$$

This permits to write,

$$\begin{aligned} V_1 &= A \begin{bmatrix} \cos\theta & -\sin\theta \\ \sin\theta & \cos\theta \end{bmatrix} \begin{bmatrix} y_2 \\ x_2 \end{bmatrix} \\ &= A \begin{bmatrix} -\sin\theta & \cos\theta \\ \cos\theta & \sin\theta \end{bmatrix} \begin{bmatrix} x_2 \\ y_2 \end{bmatrix} \\ &= A \begin{bmatrix} -\sin\theta & \cos\theta \\ \cos\theta & \sin\theta \end{bmatrix} \begin{bmatrix} \cos\theta & \sin\theta \\ -\sin\theta & \cos\theta \end{bmatrix} \begin{bmatrix} x_1 \\ y_1 \end{bmatrix} \\ &= A \begin{bmatrix} -2\sin\theta\cos\theta & -\sin\theta^2 + \cos\theta^2 \\ -\sin\theta^2 + \cos\theta^2 & 2\sin\theta\cos\theta \end{bmatrix} \begin{bmatrix} x_1 \\ y_1 \end{bmatrix} \end{aligned} \tag{1.19}$$

With the formulation of V_1 as given by Equation (1.1), it is clear that this equality is true for $\theta = -\pi/4$ and $\theta = 3\pi/4$ (meaning that V_2 is simply V_1 in a coordinate system that was rotated by either one of those two angles). As the two flows are essentially the same, the difference in the stress situations found from the analysis in the previous section can only arise from the relative orientation of the fluid element with respect to the fluid flow. If the edges of the square fluid element are parallel to the asymptotes of the flow (principal axis of the flow), only normal stresses arise, resulting in extensional strain rates. In case the edges are not aligned, shear stresses arise (with a maximum when the edges form a $45°$ angle with the flow asymptotes, where no viscous normal stresses arise). Overall, this means that the orientation of the fluid element considered is fundamental when considering stresses it experiences.

Furthermore, it can be noted that the orientation of the fluid element has no effect on the magnitude of the viscous stress components the fluid element is subjected to: in both cases, the components have a contribution of $2\mu A$, which seems to be conserved. One could think of that as a sort of "total viscous stress" which is conserved, but the relative magnitude of each component (each position in the stress tensor σ_{ij}) can change. This is similar to the use of the Mohr's circle in the mechanics of materials.

1.4 Pressure Field and Gradient of Viscous Stress Tensor

In this section, the formulation of the velocity field described by Equation (1.1) will be used. It can be shown (see White section 2-10) that an irrotational (potential) flow satisfies both the viscous and inviscid flow equations. This means that Bernoulli's equation (1.20) is valid for the flows discussed in this problem. This will first be used to determine the pressure field of the flow being analysed.

$$\rho\frac{\partial\phi}{\partial t} + p + \frac{1}{2}\rho V^2 + \rho g z = cst \tag{1.20}$$

where ϕ is the velocity potential.

1.4.1 Pressure Field

The fluid flow considered is steady: both velocity components do not depend on time (only position), meaning that the velocity potential will also be independent of time. This means that the first term in Bernoulli's equation is zero. Furthermore, gravity was neglected throughout the assignment, meaning that the fourth term of the equation can also be neglected. This reduces Bernoulli's equation to,

$$p(x,y) + \frac{1}{2}\rho V(x,y)^2 = p_0$$

where p_0 is the total pressure ($V = 0$), and $V^2 = u^2 + v^2$. This permits to write that,

$$p(x,y) = p_0 - \frac{1}{2}\,\rho A^2(x^2 + y^2) \tag{1.21}$$

This describes a pressure field which reaches a maximum at the origin, and decreases as the distance from the origin increases. All points at a distance $r = \sqrt{x^2 + y^2}$ have the same pressure (isobar), which describes a circle with a centre at the origin. A qualitative isobar plot generated from Equation (1.21), is presented in Figure 1.5.

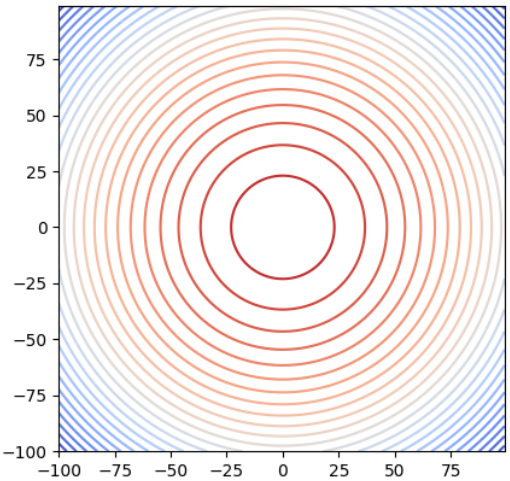

Figure 1.5: Isobars of the flow field. Warmer colours indicate a higher pressure.

1.4.2 Gradient of Viscous Stress Tensor

It was seen earlier that the viscous stress tensor can be expressed as,

$$\tau_{ij} = 2\mu\epsilon_{ij}$$

The gradient of the viscous stress tensor is then a vector given by the following. Note that for an "inviscid potential flow" (irrotational flow), the velocity potential is linked to the velocity components by: $\frac{\partial\phi}{\partial x} = u$ and $\frac{\partial\phi}{\partial y} = v$ (this was used in the third step).

$$
\begin{aligned}
\frac{\partial \tau_{ij}}{\partial x_j} &= 2\mu \frac{\partial \epsilon_{ij}}{\partial x_j} \\
&= 2\mu \begin{bmatrix} \frac{\partial^2 u}{\partial x^2} + \frac{1}{2}\left(\frac{\partial^2 u}{\partial y^2} + \frac{\partial^2 v}{\partial x \partial y}\right) \\ \frac{1}{2}\left(\frac{\partial^2 u}{\partial y \partial x} + \frac{\partial^2 v}{\partial x^2}\right) + \frac{\partial^2 v}{\partial y^2} \end{bmatrix} \\
&= 2\mu \begin{bmatrix} \frac{\partial^3 \phi}{\partial x^3} + \frac{1}{2}\left(\frac{\partial^3 \phi}{\partial y^2 \partial x} + \frac{\partial^3 \phi}{\partial x \partial y^2}\right) \\ \frac{1}{2}\left(\frac{\partial^3 \phi}{\partial y \partial x^2} + \frac{\partial^3 \phi}{\partial x^2 \partial y}\right) + \frac{\partial^3 \phi}{\partial y^3} \end{bmatrix} \\
&= 2\mu \begin{bmatrix} \frac{\partial^3 \phi}{\partial x^3} + \frac{\partial^3 \phi}{\partial x \partial y^2} \\ \frac{\partial^3 \phi}{\partial x^2 \partial y} + \frac{\partial^3 \phi}{\partial y^3} \end{bmatrix} \\
&= 2\mu \begin{bmatrix} \frac{\partial}{\partial x}\left(\frac{\partial^2 \phi}{\partial x^2} + \frac{\partial^2 \phi}{\partial y^2}\right) \\ \frac{\partial}{\partial y}\left(\frac{\partial^2 \phi}{\partial x^2} + \frac{\partial^2 \phi}{\partial y^2}\right) \end{bmatrix}
\end{aligned}
$$

Furthermore, from the continuity equation, the following can be noted,

$$
\begin{aligned}
\frac{\partial u}{\partial x} + \frac{\partial v}{\partial y} &= 0 \\
\Leftrightarrow \frac{\partial^2 \phi}{\partial x^2} + \frac{\partial^2 \phi}{\partial y^2} &= 0 = \Delta \phi
\end{aligned}
$$

Therefore, the gradient of the viscous stress tensor of an inviscid potential is the zero vector,

$$
\frac{\partial \tau_{ij}}{\partial x_j} = \vec{0} \tag{1.22}
$$

This shows that although the viscous stresses are not zero, the gradient of the viscous tensor is a zero vector. However, in the case of an incompressible flow field (decoupling of the energy equation from the continuity and momentum equations), the viscous effects only arise in the momentum equations through the gradient of the viscous stresses tensor,

$$
\rho \frac{Du_i}{Dt} = -\frac{\partial p}{\partial x_i} + \frac{\partial \tau_{ij}}{\partial x_j} \tag{1.23}
$$

As the gradient of the viscous stress tensor is a zero vector, the effect of viscosity is not present in the viscous equations. Therefore, the "inviscid potential flow" satisfies both the inviscid (obviously) and the viscous equations (Navier-Stokes incompressible).

Problem 2.C – Stagnation Flow on an Infinite Swept Wing 2

In the following, two different coordinate systems will be used to analyse the stagnation flow on an infinite swept wing case, based on the numerical solution provided in the assignment. The coordinate systems were provided in slide deck 2B, and are repeated in Figure 2.1. Therefore, The x-direction is the chord-wise (u velocity), the y-direction is the wall normal (v velocity), and the z-direction is the span-wise (w velocity), direction. The solution is assumed to be invariant in the span-wise z-direction, and the boundary conditions are the following: no slip at the wall ($y = 0 : u = v = w = 0$), and the u and w components tend to the external flow when y tends to infinity ($y \to +\infty : u \to u_e; w \to w_e$). Furthermore, Equations (2.1) and (2.2) give the definitions of F and g, functions relating the normalised (with respect to the external flow velocity components u_e and w_e) velocity components in the boundary layer, to η, the self-similar variable.

$$\frac{u}{u_e} = F'(\eta) \tag{2.1}$$

$$\frac{w}{w_e} = g(\eta) \tag{2.2}$$

From those definitions, we conclude (as will be useful later in this problem) that F"(0) and g'(0) (given in the assignment) are related to the gradients of u and w at the wall. Having laid out the context of the assignment in terms of the used coordinate systems and variables, the following sections provide the answers to the questions given in the problem definition.

2.1 Velocity Profiles and Cross-Flow Angle

First, the velocity components u and w are normalised by $u_{se} = \sqrt{u_e^2 + w_e^2}$, defining $r = \frac{w_e}{u_e}$,

$$u_{se} = u_e\sqrt{1 + r^2} \tag{2.3}$$

$$u_{se} = w_e\sqrt{1 + \left(\frac{1}{r}\right)^2} \tag{2.4}$$

The velocity components normalised by u_{se} are then obtained from,

$$\frac{u}{u_{se}} = \frac{u}{u_e}\frac{1}{\sqrt{1 + r^2}} \tag{2.5}$$

$$\frac{w}{w_{se}} = \frac{w}{w_e}\frac{1}{\sqrt{1 + \left(\frac{1}{r}\right)^2}} \tag{2.6}$$

To obtain the velocity components with respect to the flow direction, as defined in Figure 2.1b, Equations (2.7) (streamwise direction) and (2.8) (cross-flow direction) are used, as given on slide 2b-21. Note that the absolute external flow direction, ϕ_e, is given by $\tan\phi_e = \frac{w_e}{u_e} = r$.

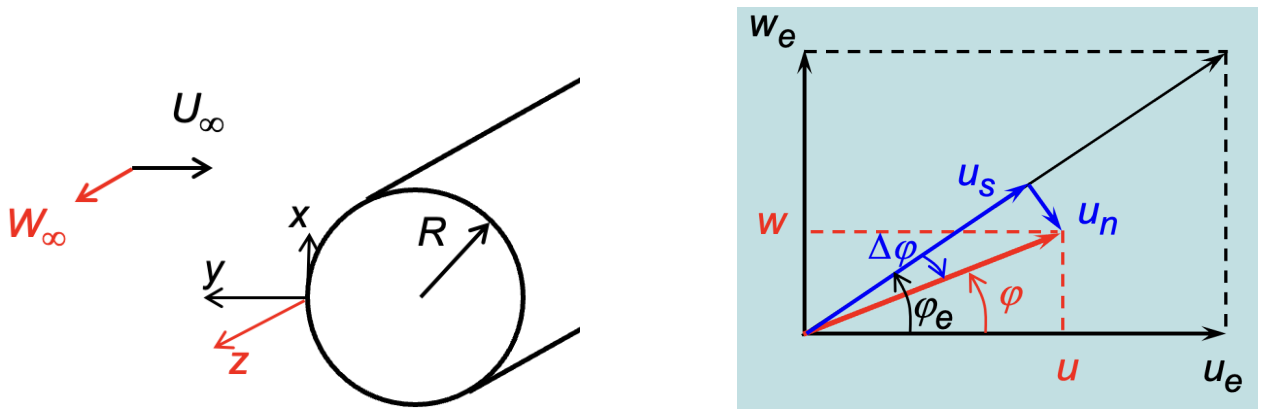

(a) Coordinate system with respect to the wing geometry, used for problem 2.C, as given on slide 2b-18.

(b) Coordinate system defined with respect to the external flow, used for problem 2.C, as given on slide 2b-21.

Figure 2.1: Coordinate systems used in the rest of the solution of problem 2.C.

$$\frac{u_s}{u_{se}} = \frac{u}{u_{se}}\cos\phi_e + \frac{w}{u_{se}}\sin\phi_e \tag{2.7}$$

$$\frac{u_n}{u_{se}} = \frac{u}{u_{se}}\sin\phi_e - \frac{w}{u_{se}}\cos\phi_e \tag{2.8}$$

Finally, the cross-flow angle is computed using $\Delta\phi = \arctan\left(\frac{u_n/u_{se}}{u_s/u_{se}}\right)$. However, a special case needs to be handled at the wall ($\eta = 0$), where both components are zero. To handle this case, the gradients of the velocity components are used, as shown in Equation (2.9), giving the cross-flow angle at the wall. Note that the conversion factors from the normalisation by u_e and w_e are both constants. Additionally, from the definitions provided by Equations (2.1) and (2.2), $F''(\eta) = \frac{\partial(u/u_e)}{\partial\eta}$ and $g'(\eta) = \frac{\partial(w/w_e)}{\partial\eta}$.

$$\begin{aligned}
\Delta\phi|_w &= \phi_e - \phi \\
&= \phi_e - \arctan\left(\frac{\frac{\partial(w/u_{se})}{\partial\eta}|_w \cdot \Delta\eta}{\frac{\partial(u/u_{se})}{\partial\eta}|_w \cdot \Delta\eta}\right) \\
&= \phi_e - \arctan\left(\frac{\frac{\partial(w/w_e)}{\partial\eta}|_w \frac{1}{\sqrt{1+\left(\frac{1}{r}\right)^2}} \cdot \Delta\eta}{\frac{\partial(u/u_e)}{\partial\eta}|_w \frac{1}{\sqrt{1+r^2}} \cdot \Delta\eta}\right) \\
&= \phi_e - \arctan\left(\frac{g'(0)\frac{1}{\sqrt{1+\left(\frac{1}{r}\right)^2}}}{F''(0)\frac{1}{\sqrt{1+r^2}}}\right)
\end{aligned} \tag{2.9}$$

The profiles of the normalised velocity components (by u_{se}) are given by Figure 2.2. Additionally, a hodograph of those components is provided by Figure 2.3, and the cross-flow angle profile is given by Figure 2.4 (given $F''(0) = 1.23259$ and $g'(0) = 0.57047$). It is clear that the velocity profiles u_s and u_n have boundary layer like development (meaning that the overall velocity profile will have a boundary layer like development). Furthermore, it can be seen in the u_n profile that the velocity component perpendicular to the external velocity direction is the largest at a value of $\eta \approx 1$. Additionally, it can be noted that the cross-flow angle reaches a maximum at the wall in a nearly linear fashion towards the end of the profile.

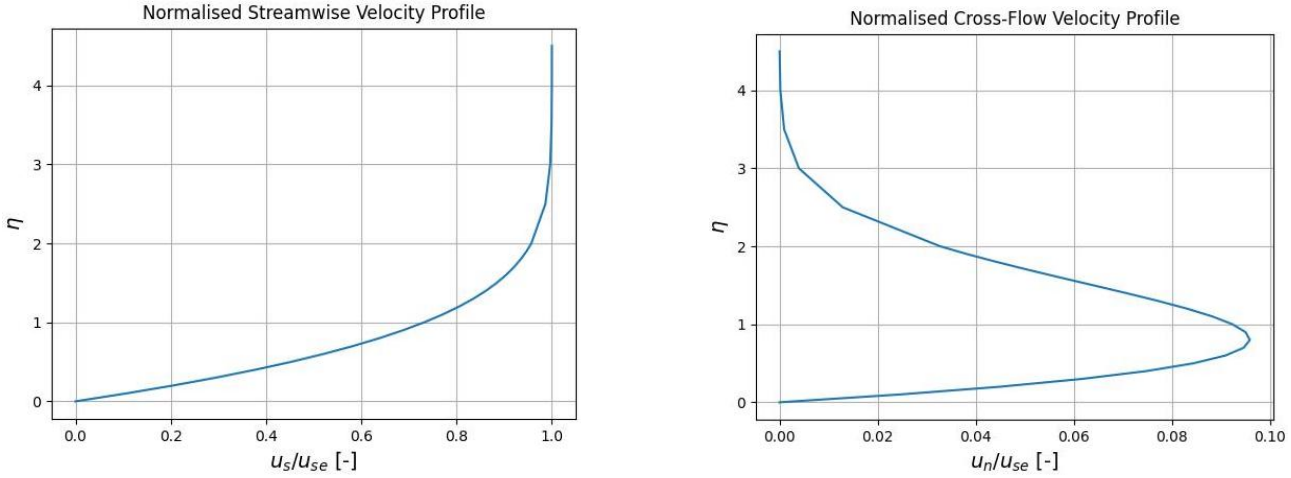

(a) u_s/u_{se} profile.

(b) u_n/u_{se} profile.

Figure 2.2: Normalised velocity profiles in the external flow aligned coordinate system.

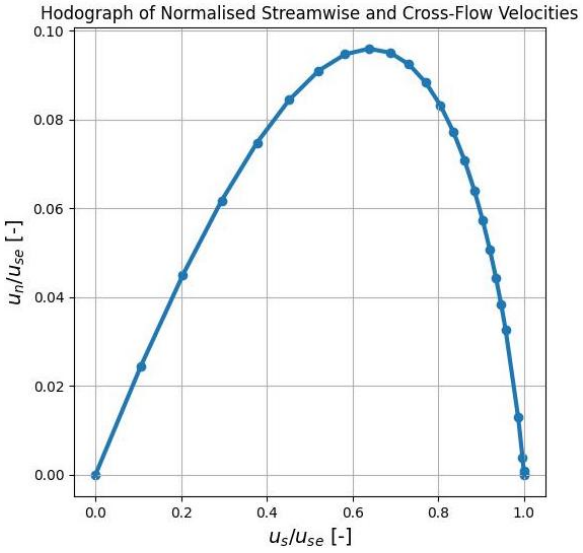

Figure 2.3: Hodograph of the normalised velocity components.

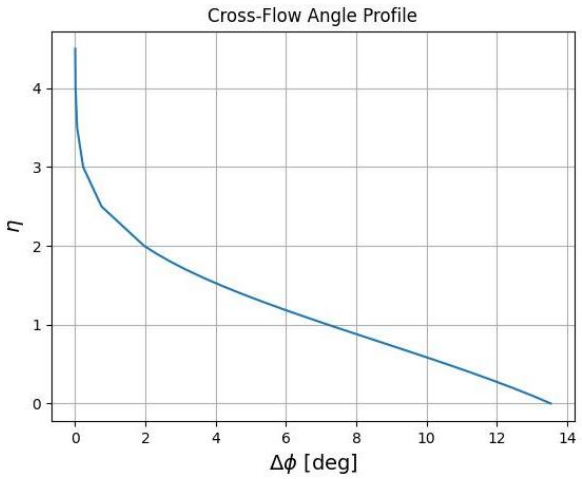

Figure 2.4: Cross flow angle profile.

2.2 Maximum Cross-Flow Angle

Following, the general expression for the cross-flow angle at the wall, $\Delta\phi_w$, as a function of $r = \frac{w_e}{u_e}$ was already nearly completely given in Equation (2.9). Rewriting the expression to simplify the square roots in the second term of the final version of the expression, and plugging in the expression of the external flow angle, Equation (2.10) is obtained (assuming $r \geq 0$).

$$\begin{aligned}
\Delta\phi|_w &= \phi_e - \arctan\left(\frac{g'(0)\frac{1}{\sqrt{1+\left(\frac{1}{r}\right)^2}}}{F''(0)\frac{1}{\sqrt{1+r^2}}}\right) \\
&= \arctan(r) - \arctan\left(\frac{g'(0)}{F''(0)}\sqrt{\frac{(1+r^2)r^2}{r^2+1}}\right) \\
&= \arctan(r) - \arctan\left(\frac{g'(0)}{F''(0)}r\right)
\end{aligned} \tag{2.10}$$

The maximum of cross-flow angle can be obtained by taking the derivative of this expression with respect to r, and setting to zero (only a maximum can be obtained as the $\arctan x$ function is monotonously increasing for increasing x, which is the case as neither g'(0) or F"(0) is negative). Setting $k = \frac{g'(0)}{F''(0)}$ for convenience,

$$\frac{d(\Delta\phi|_w)}{dr} = \frac{1}{1+r^2} - \frac{1}{1+k^2r^2}k = 0 \tag{2.11}$$

which can be solved as followed,

$$\begin{aligned}
&\frac{1}{1+r^2} - \frac{1}{1+k^2r^2}k = 0 \\
\Leftrightarrow\ &1 + k^2r^2 - (1+r^2)k = 0 \\
\Leftrightarrow\ &r^2(k^2-k) + (1-k) = 0 \\
\Leftrightarrow\ &-r^2k(1-k) + (1-k) = 0 \\
\Leftrightarrow\ &r^2 = \frac{1}{k}
\end{aligned}$$

Solving for r yields, $\frac{w_e}{u_e} = \sqrt{\frac{F''(0)}{g'(0)}} \approx 1.4699$ (assuming only positive values of r are possible, although a similar minimum would be reached as the expression is odd). This value of r is associated to a cross-flow angle of 21.544°.

2.3 Python Code - Problem 2.C

The following code was used to answer question 2.C-a.

```
import numpy as np
import csv
import matplotlib.pyplot as plt
from metpy.plots import Hodograph
def read_CSV(file):
    '''

    :param file:
    :return:
    '''
    with open(file, 'r') as file:
        csvreader = csv.reader(file)
        csv_headings = next(csvreader)
        first_line = next(csvreader)
        first_line = [float(i) for i in first_line]
        data = np.array(first_line)
        for row in csvreader:
            row = [float(i) for i in row]
            data = np.vstack((data, row))
    return data

### Main code
if '__main__':
    # External flow data
    we_ue = 1.4699
    phi_e = np.arctan(we_ue)  # rad

    # Data at the wall
    Fpp_w = 1.23259  # proxy for du/dy at the wall
    gpp_w = 0.57047  # proxy for dw/dy at the wall

    # Get data from CSV file
    BL_data = read_CSV(f'./Data')
    eta = BL_data[:, 0]

    # Normalise the BL data to the outer flow u_se
    ## Obtain the normalisation coefficients
    fu_use = np.sqrt(1+we_ue**2)
    fw_use = np.sqrt(1+we_ue**(-2))

    ## Normalise the data by applying the coefficients
    u_BL = BL_data[:, 1]/fu_use
    w_BL = BL_data[:, 2]/fw_use
    Fpp_w_n = Fpp_w/fu_use
    gpp_w_n = gpp_w/fw_use

    # Decompose the u-w velocities to the us-un system (wrt to the external flow velocity
     vector)
    us = u_BL * np.cos(phi_e) + w_BL * np.sin(phi_e)
    un = u_BL * np.sin(phi_e) - w_BL * np.cos(phi_e)

    # cross-flow angle
    ## At the wall
    phi_w = np.arctan2(gpp_w_n, Fpp_w_n)
    dphi_w = np.rad2deg(phi_e - phi_w)

    ## Everywhere else
    dphi = np.rad2deg(phi_e - np.arctan2(w_BL, u_BL))  # np.rad2deg(np.arctan2(un, us))
    dphi[0] = dphi_w

    plt.figure(1)
    plt.plot(us, eta)
```

```
    plt.title('Normalised Streamwise Velocity Profile')
    plt.xlabel(r"$u_{s} / u_{se}$ [-]", fontsize=14)
    plt.ylabel(r'$\eta$', fontsize=14)
    plt.grid(True)
    #plt.savefig(f'./us_prof.jpg')

    plt.figure(2)
    plt.plot(un, eta)
    plt.title('Normalised Cross-Flow Velocity Profile')
    plt.xlabel(r"$u_{n} / u_{se}$ [-]", fontsize=14)
    plt.ylabel(r'$\eta$', fontsize=14)
    plt.grid(True)
    #plt.savefig(f'./un_prof.jpg')

    plt.figure(3)
    plt.plot(dphi, eta)
    plt.title('Cross-Flow Angle Profile')
    plt.xlabel(r"$\Delta \phi$ [deg]", fontsize=14)
    plt.ylabel(r'$\eta$', fontsize=14)
    plt.grid(True)
    #plt.savefig(f'./phi_prof.jpg')

    plt.figure(4, figsize=(6, 6))
    plt.plot(us, un, linewidth=3)
    plt.scatter(us, un)
    plt.title('Hodograph of Normalised Streamwise and Cross-Flow Velocities')
    plt.xlabel(r"$u_{s} / u_{se}$ [-]", fontsize=14)
    plt.ylabel(r"$u_{n} / u_{se}$ [-]", fontsize=14)
    plt.grid(True)
    #plt.savefig(f'./hodo.jpg')

    r = np.arange(-2, 2, 0.001)
    dphi_max = np.rad2deg(np.arctan(r) - np.arctan2(gpp_w*r, Fpp_w))
    plt.figure(5)
    plt.plot(r, dphi_max)
    plt.grid(True)
    plt.show()
```

Listing 2.1: Problem 2.C Python code

Problem 3.F – Similar Expansion Boundary Layer $\beta = -1$

3

This problem considers the Falkner-Skan (F-S) equation (3.1), which describes the self-similar boundary solutions which are obtained for pressure distribution corresponding with external flows of the form $u_e(x)\ x^m$.

$$f''' + ff'' + \beta(1 - (f')^2) = 0 \tag{3.1}$$

With, $\frac{u}{u_e} = f'(\eta)$, $\eta = \frac{y}{x}\sqrt{\frac{m+1}{2}\frac{u_e x}{\nu}}$, and $\beta = \frac{2m}{m+1}$. In the present case, no-slip and a non-zero normal velocity are used as boundary conditions at the wall:

$$\begin{aligned} f'(0) &= 0 \\ f(0) = f_w &= \frac{-v_w}{u_e}\sqrt{\frac{2}{m+1}\frac{u_e x}{\nu}} \end{aligned} \tag{3.2}$$

Additionally, a solution showing a boundary layer character is one exhibiting the behaviour: $\eta \to +\infty : f'(\eta) = 1$. For the geometry analysed below, $f_w = 0$ would result in flow separation, which cannot be analysed through the F-S equation, meaning that suction (positive f_w) is necessary to ensure a boundary layer solution. In general, due to the non-linear character of the F-S equation, not all combinations of negative β and f_w allows a solution which possesses a boundary layer character. Additionally, some other combinations may display multiple solutions.

Having laid down the context of the assignment, the answers to the questions provided in the assignment are given in the following sections.

3.1 Expansion Geometry

The Falkner-Skan equation in this form describes a family of similarity solutions, which are the **wedge flows**. $\beta = -1$ then refers to an expansion right angle (90°downard deflection of the flow), as shown in Figure 3.1. Furthermore, this geometry corresponds to the external flow $u_e(x) = Kx^{-1/3}$ (by solving $\beta = -1 = \frac{2m}{m+1}$).

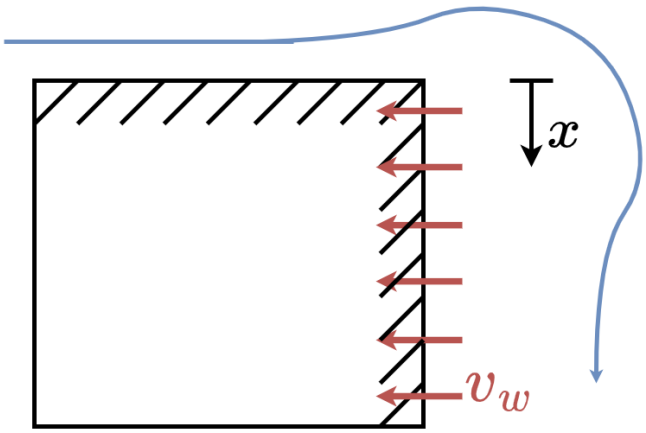

Figure 3.1: Expansion geometry for $\beta = -1$, from slide 3a-24. Note that v_w is given in its negative direction here, for a positive f_w.

3.2 Analytical Integration

For the considered situation of $\beta = -1$, the F-S equation can be integrated twice analytically, which permits to introduce the integration constants f_w and f''_w, characterising the flow at the wall. Starting from,

$$f''' + ff'' + f'f' = 1$$

The second and third terms on the left hand side can be written as $ff'' + f'f' = \frac{\partial(ff')}{\partial\eta}$, such that,

$$f''' + \frac{\partial(ff')}{\partial\eta} = 1$$

Integrating a first time results in,

$$f'' + ff' = \eta + C_1 \tag{3.3}$$

Evaluating Equation (3.3) at the wall, where $\eta = 0$ and $f'(0) = 0$, results in $C_1 = f''_w$. Following, $ff' = f\frac{\partial f}{\partial\eta} = \frac{1}{2}\frac{\partial f^2}{\partial\eta}$ permits to rewrite the Equation (3.3) and integrate a second time the expression,

$$f' + \frac{f^2}{2} = \frac{\eta^2}{2} + f''_w\eta + C_2$$

Again evaluating the expression at the wall, for $\eta = 0$ and $f'(0) = 0$, yields, $C_2 = \frac{f_w^2}{2}$. The twice integrated Falkner-Skan equation for the case of $\beta = -1$ is then given by Equation (3.4).

$$f' + \frac{f^2}{2} = \frac{\eta^2}{2} + f''_w\eta + \frac{f_w^2}{2} \tag{3.4}$$

3.3 Boundary Layer Behaviour of the Solution

From the derivation above, two new forms of the F-S equation were found, as given by Equation (3.5).

$$\begin{cases} f'' + ff' = \eta + f''_w \\ f' + \frac{f^2}{2} = \frac{\eta^2}{2} + f''_w\eta + \frac{f_w^2}{2} \end{cases} \tag{3.5}$$

A solution is said to have a boundary layer character if $\eta \to +\infty : f'(\eta) = 1$, which also implies that $\eta \to +\infty : f'' \to 0$ (if the slope of f tends towards a constant, its curvature tends towards zero). Evaluating the two expressions of Equation (3.5) for $\lim_{\eta\to+\infty}$,

$$\begin{cases} f = \eta + f''_w \\ 1 + \frac{f^2}{2} = \frac{\eta^2}{2} + f''_w\eta + \frac{f_w^2}{2} \end{cases} \tag{3.6}$$

Writing, $\frac{f^2}{2} = \frac{1}{2}(\eta + f''_w)^2 = \frac{1}{2}(\eta^2 + 2\eta f''_w + f''^2_w)$ from the first expression and replacing $\frac{f^2}{2}$ in the second yields, $\frac{\eta^2}{2} + \eta f''_w + \frac{f''^2_w}{2} + 1 = \frac{\eta^2}{2} + f''_w\eta + \frac{f_w^2}{2}$. Resulting in Equation (3.7)

$$f''^2_w = f_w^2 - 2 \tag{3.7}$$

It can therefore be concluded that, for a boundary layer character of the solution to arise, $f''^2_w = f_w^2 - 2$. This shows that only values of f_w which are larger than $f_{w_{lp}} = \sqrt{2}$ (otherwise f''_w, which is a physical quantity, would need to be an imaginary number) provide sufficient suction for a boundary layer to form on the wall. Note that negative values of f_w are not considered as v_w is negative in Equation (3.2), for the case considered.

Following the displacement thickness, δ^*, of the boundary layer (for cases satisfying the previously mentioned requirements to yield a boundary layer character), is obtained from its definition given by Equation (3.8). Note that $dy = d\eta x\sqrt{\frac{2\nu}{(m+1)u_e(x)x}}$, and $\lim_{\eta\to+\infty} f(\eta) = \eta + f''_w$ from the first expression of Equation (3.6).

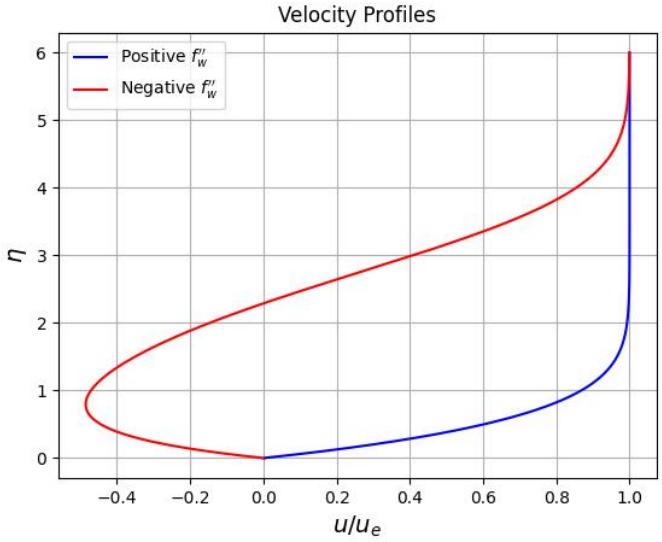

Figure 3.2: Velocity profiles for $f''_w \geq 0$ and $f''_w \leq 0$.

$$\begin{aligned}
\delta^* &= \int_0^{+\infty} \left(1 - \frac{u}{u_e}\right) dy = \int_0^{+\infty} \left(1 - f'(\eta)\right) x \sqrt{\frac{2\nu}{(m+1)u_e(x)x}} d\eta \\
&= \lim_{t \to +\infty} x \sqrt{\frac{2\nu}{(m+1)u_e(x)x}} \left[\eta - f(\eta)\right]_0^t \\
&= x \sqrt{\frac{2\nu}{(m+1)u_e(x)x}} \lim_{t \to +\infty} \left(t - f(t) - (0 - f(0))\right) \\
&= x \sqrt{\frac{2\nu}{(m+1)u_e(x)x}} \lim_{t \to +\infty} \left(t - t - f''_w + f_w\right)
\end{aligned} \tag{3.8}$$

Plugging $u_e = Kx^{-1/3}$ and $m = \frac{-1}{3}$, the displacement thickness can be written as Equation (3.9).

$$\delta^* = (f_w - f''_w) x \sqrt{\frac{2\nu}{(m+1)u_e(x)x}} = (f_w - f''_w) \sqrt{\frac{3\nu x^{4/3}}{K}} \tag{3.9}$$

It can be seen that the displacement thickness is as expected, a function of the x position. Furthermore, as already seen from Equation (3.7) derived earlier, $f_w \geq f''_w$ (only positive values of f_w are considered) for the boundary layer to form (physical meaning for $\delta^* \geq 0$ only).

3.4 Velocity Profile for $f_w = 2.25$

Taking $f_w = 2.25$, Equation (3.7) yields that $f''_w = 1.75$ or $f''_w = -1.75$. Those values, coupled with $f'(0) = 0$, permit to integrate Equation (3.1) using a numerical method such as the 4th order Runge Kutta method (RK4), to march in space from $\eta = 0$. The third order differential equation can be decoupled into a system of three 1st order Ordinary Differential Equation, as given below. This system can directly be fed to the classical RK4 implementation to solve the differential equation. Note that the original version of the equation was used, and not the already twice integrated one (as this version was as straightforward to implement).

$$F_i = \begin{bmatrix} F_1 \\ F_2 \\ F_3 \end{bmatrix} = \begin{bmatrix} f \\ f' \\ f'' \end{bmatrix} \qquad F'_i = \begin{bmatrix} f' \\ f'' \\ f''' \end{bmatrix} = \begin{bmatrix} F_2 \\ F_3 \\ 1 - F_2 F_2 - F_1 F_3 \end{bmatrix}$$

This system results in the velocity profiles shown in Figure 3.2, which shows the two feasible solutions for the case considered. Both profiles result in a boundary layer character of the velocity profile (they both converge to the external flow), but the solution arising from $f''_w \leq 0$ shows flow reversal near the wall. As expected from the introduction of the problem, two solutions for $\beta = -1$ and a given value of f_w are found.

3.5 Python Code - Problem 3.F

```python
import numpy as np
import matplotlib.pyplot as plt

def dF(y, eta):
    return np.array([y[1], y[2], 1 - y[1]**2 - y[0]*y[2]])

def RK4(y0):
    deta = 0.001
    eta = 0
    y_list = y0
    eta_list = [0]

    y = y0
    while eta < 6:
        k1 = dF(y, eta)
        k2 = dF(y + k1 * (deta / 2), eta + deta / 2)
        k3 = dF(y + k2 * (deta / 2), eta + deta / 2)
        k4 = dF(y + k3 * deta, eta + deta)

        y += deta * (k1 + 2 * k2 + 2 * k3 + k4) / 6
        y_list = np.vstack((y_list, y))
        eta += deta
        eta_list.append(eta)
    return y_list, eta_list

# Assignment variables
fw = 2.25
fppw1 = np.sqrt(fw**2 - 2)
fppw2 = -np.sqrt(fw**2 - 2)

# Initial conditions
f0 = fw
fp0 = 0
fpp0_1 = fppw1
fpp0_2 = fppw2

# Define derivative function for RK4

# RK4
y01 = np.array([f0, fp0, fpp0_1])
y_list1, eta_list1 = RK4(y01)

y02 = np.array([f0, fp0, fpp0_2])
y_list2, eta_list2 = RK4(y02)

plt.figure(1)
plt.plot(y_list1[:, 1], eta_list1, 'b', label=r"Positive $f_{w}''$")
plt.plot(y_list2[:, 1], eta_list2, 'r', label=r"Negative $f_{w}''$")
plt.legend()
plt.ylabel(r'$\eta$', fontsize=14)
plt.xlabel(r'$u / u_{e}$', fontsize=14)
plt.title('Velocity Profiles')
plt.grid(True)
plt.savefig(f'./VelocityProfile3.jpg')
plt.show()

print(fppw1, fppw2)
```

Listing 3.1: Problem 3.F Python code

Problem 4.E – Flat Plate Boundary Layer with Uniform Suction – Integral Method

4

This problem considers an integral method analysis of the boundary layer flow on a flat plate with uniform suction ($u_e(x) = U_\infty = cst$ and $v_w = cst < 0$). Such boundary layer flow displays a non-similar development, and is represented in Figure 4.1

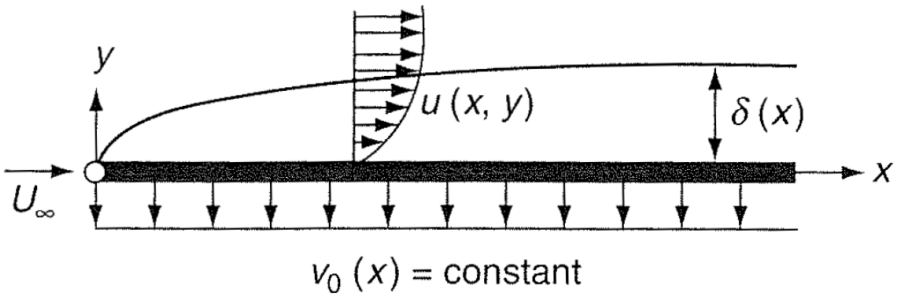

Figure 4.1: Boundary layer flow on a flat plate with uniform suction.

Two asymptotic behaviours can be distinguished:

1. Towards the Leading Edge (LE), the BL behaviour like the Blasius solution with,

$$\frac{\theta}{x} = \frac{2\tau_w}{\rho U_\infty^2} = 0.66411\sqrt{\frac{\nu}{U_\infty x}} \tag{4.1}$$

2. Further away from the LE (at larger distances downstream), the boundary layer develops towards a uniform suction profile with,

$$\frac{u(\eta)}{U_\infty} = 1 - e^{-\eta} \qquad \eta = \frac{(-v_w)y}{\nu} \tag{4.2}$$

In this problem, an integral analysis of the problem is performed to compute an approximate development of the boundary layer development (and especially the momentum thickness θ). Under the prescribed conditions, the integral momentum equation is given by Equation (4.3), with $S = \frac{\tau_w \theta}{\mu U_\infty}$ and $\theta(x = 0) = 0$. Note that the shear-parameter S is only a function of the shape of the velocity profile and not its thickness.

$$\frac{U_\infty}{2\nu}\frac{d\theta^2}{dx} = \frac{\tau_w \theta}{\mu U_\infty} + \frac{v_w \theta}{\nu} = S + \frac{v_w \theta}{\nu} \tag{4.3}$$

Having the context of the problem, the following sections tackle the different questions of the problem.

4.1 Coordinate Scaling

4.1.1 Integral Momentum Relation

Defining,

$$\xi = x\frac{v_w^2}{\nu U_\infty} \quad \Leftrightarrow x = \xi\frac{\nu U_\infty}{v_w^2} \tag{4.4}$$

$$\theta^* = \theta\frac{-v_w}{\nu} \quad \Leftrightarrow \theta = \theta^*\frac{\nu}{-v_w} \tag{4.5}$$

Inserting in Equation (4.3),

$$\frac{U_\infty}{2\nu}\frac{d\left(\frac{\nu^2}{v_w^2}(\theta^*)^2\right)}{d\left(\xi\frac{\nu U_\infty}{v_w^2}\right)} = S + \frac{v_w}{\nu}\theta^*\frac{\nu}{-v_w}$$

Which simplifies to Equation (4.6), the requested result. This is a simpler form of the integral momentum relation, obtained from the conveniently used scaling. Note that the boundary conditions of θ at $x = 0$ translate directly (from the coordinate transformation given above) to $\theta^*(\xi = 0) = 0$.

$$\frac{d(\theta^*)^2}{d\xi} = 2(S - \theta^*) \tag{4.6}$$

4.1.2 Asymptotic Behaviour

From the exact (theoretical) solutions of the Blasius and uniform suction profiles, the asymptotic solutions of θ^* for small and large ξ's can be obtained by applying the coordinate scaling to Equations (4.1) and (4.2). First considering the Blasius solution at small x and ξ. Note that $\sqrt{v_w^2} = -v_w$ as $v_w < 0$, and Equation (4.1) can be written as $\theta = 0.66411\sqrt{\frac{\nu x}{U_\infty}}$.

$$\begin{aligned}
\theta^* &= \theta\frac{-v_w}{\nu} \\
&= 0.66411\sqrt{\frac{\nu\left(\xi\frac{\nu U_\infty}{v_w^2}\right)}{U_\infty}}\left(\frac{-v_w}{\nu}\right) \\
&= 0.66411\frac{\nu}{(-v_w)}\frac{-v_w}{\nu}\sqrt{\xi} \\
&= 0.66411\sqrt{\xi}
\end{aligned}$$

Therefore, the solution behaves like Equation (4.7) close to the LE. This was expected as the Blasius solution dictates a square root like development of the boundary layer on a flat plate.

$$\theta^* = 0.66411\sqrt{\xi} \tag{4.7}$$

Plugging into Equation (4.6) and taking $\lim_{\xi\to 0}$, the equation below is obtained. Meaning that the solution is in agreement with the integral momentum equation if S takes the value $\frac{(0.66411)^2}{2}$. This will be seen to be the case for small ξ in the following section. Therefore, the solution in the $\theta^* - \xi$ plane goes towards zero with a slope of $(0.66411)^2$ for $\xi \to 0$.

$$\begin{aligned}
\lim_{\xi\to 0}(0.66411)^2\frac{d\xi}{d\xi} &= \lim_{\xi\to 0} 2(S - 0.66411\sqrt{\xi})) \\
\Leftrightarrow S &= \frac{(0.66411)^2}{2}
\end{aligned}$$

Similarly, the asymptotic solution of θ^* for large ξ is obtained by applying the coordinate scaling to the uniform suction velocity profile, as given below. Note that $\eta = y\frac{-v_w}{\nu}$, therefore, $dy = d\eta(\frac{\nu}{-v_w})$, and the definition of θ is used with f being the velocity profile scaled by the external flow velocity.

$$\begin{aligned}
\theta^* &= \theta\frac{-v_w}{\nu} \\
&= \frac{-v_w}{\nu}\int_0^{+\infty} f(y)(1 - f(y))dy \\
&= \frac{-v_w}{\nu}\int_0^{+\infty} f(\eta)(1 - f(\eta))\frac{\nu}{-v_w}d\eta
\end{aligned}$$

$$
\begin{aligned}
&= \int_0^{+\infty} (1 - e^{-\eta}) e^{-\eta} d\eta \\
&= \int_0^{+\infty} (e^{-\eta} - e^{-2\eta}) d\eta \\
&= \lim_{t \to +\infty} \left[-e^{-\eta} + \frac{1}{2} e^{-2\eta} \right]_0^t \\
\theta^* &= (0 + 0 - (-1 + \frac{1}{2})) = \frac{1}{2}
\end{aligned}
$$

Plugging this result in Equation (4.6), the asymptotic solution is in agreement with the equation if $S = \frac{1}{2}$, which will be seen to be the case for large ξ in the following section. Furthermore, this means that the boundary layer reaches $\theta^* = \frac{1}{2}$ asymptotically for $\xi \to +\infty$, with a slope of 0 (at infinity).

4.2 Value of S

The value of S is not a constant, and changes throughout the boundary layer development. However, a first estimate can be obtained by considering a constant value of S derived from either the Blasius or uniform suction exact solutions provided by Equations (4.1) and (4.2). First, those values for S are derived, then the accuracy of the method is discussed through comparison with a Finite-Difference scheme provided in the assignment.

4.2.1 Blasius Solution S

As previously given, the definition of the shear parameter is $S = \frac{\tau_w \theta}{\mu U_\infty}$. In the previous section, θ^* was found to be $\theta^* = 0.66411\sqrt{\xi}$ for the Blasius solution. Therefore,

$$\theta = \theta^* \frac{\nu}{-v_w} = 0.66411 \sqrt{\xi} \frac{\nu}{-v_w}$$

Following, the shear stress at the wall is given by Equation (4.1) to be,

$$
\begin{aligned}
\tau_w &= \frac{\rho U_\infty^2}{2} 0.66411 \sqrt{\frac{\nu}{U_\infty x}} \\
&= \frac{\rho U_\infty^2}{2} 0.66411 \sqrt{\frac{\nu}{U_\infty \xi \frac{\nu U_\infty}{v_w^2}}} \\
&= \frac{\rho U_\infty}{2} 0.66411 (-v_w) \sqrt{\frac{1}{\xi}}
\end{aligned}
$$

Combining those results in Equation (4.8), with $\nu = \frac{\mu}{\rho}$. Note that this is consistent with the previous conclusions on the required value of S for small values of ξ in the previous section.

$$S = \frac{\tau_w \theta}{\mu U_\infty} = \frac{1}{\mu U_\infty} \frac{\rho U_\infty}{2} 0.66411 (-v_w) \sqrt{\frac{1}{\xi}} 0.66411 \sqrt{\xi} \frac{\nu}{-v_w} = \frac{(0.66411)^2}{2} \tag{4.8}$$

4.2.2 Uniform Suction Solution S

Similarly, the value of S resulting from the uniform suction solution can be obtained. In the previous section it was found that θ^* has the value $\theta^* = \frac{1}{2}$ for the uniform suction solution. Therefore,

$$\theta = \theta^* \frac{\nu}{-v_w} = \frac{1}{2} \frac{\nu}{-v_w}$$

Following, the shear stress at the wall is given by,

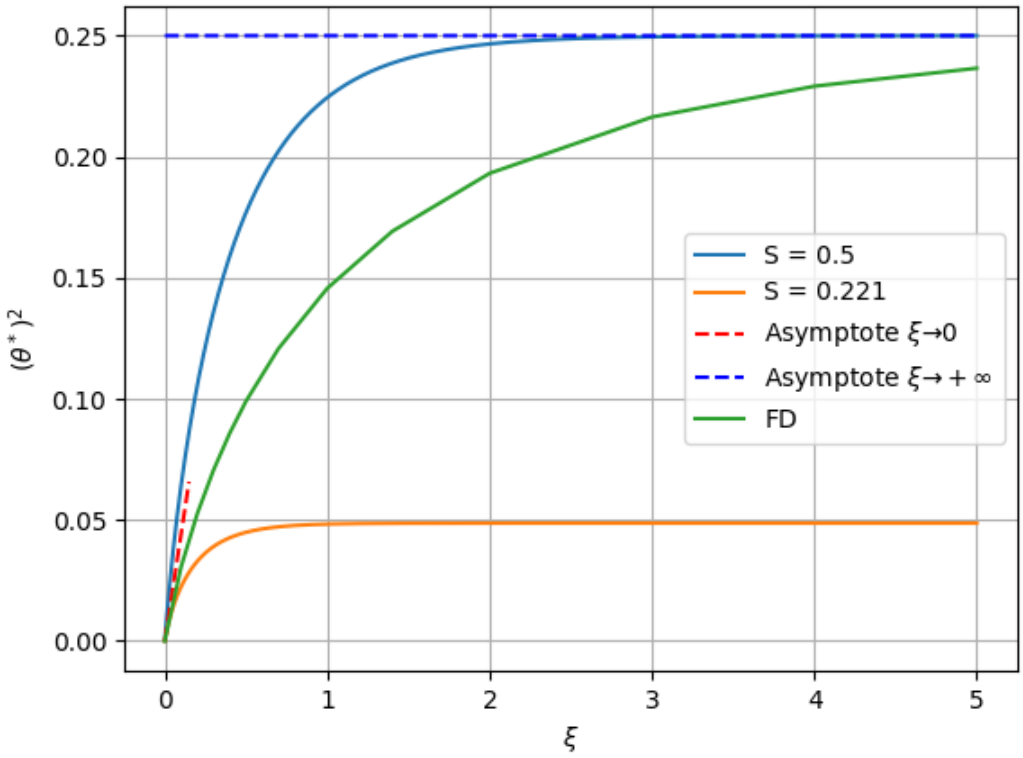

Figure 4.2: The BL development according to Equation (4.6) for different constant S values, compared to the Finite Difference solution. The asymptotes of the solution are also given in dashed lines.

$$
\begin{aligned}
\tau_w &= \mu \frac{\partial u}{\partial y}|_{y=0} \\
&= \mu \frac{\partial}{\partial y}\left(U_\infty \left(1 - e^{\frac{y v_w}{\nu}}\right)\right)|_{y=0} \\
&= -\mu U_\infty \frac{v_w}{\nu} e^{\frac{y v_w}{\nu}}|_{y=0} \\
\tau_w &= -\mu U_\infty \frac{v_w}{\nu}
\end{aligned}
$$

Combining results in Equation (4.9),

$$S = \frac{\tau_w \theta}{\mu U_\infty} = -\mu U_\infty \frac{v_w}{\nu} \frac{1}{2} \frac{\nu}{-v_w} \frac{1}{\mu U_\infty} = \frac{1}{2} \tag{4.9}$$

Note that this is also consistent with the conclusion on the required value of S for large ξ from the previous section.

4.2.3 Numerical Results and Discussion

Equation (4.6) was integrated numerically using the Runge-Kutta 4th order explicit scheme in the form $\frac{dm}{d\xi} = 2(S - \sqrt{m})$, where $m = \theta^{*^2}$ (θ^* can only be positive in this case), and with steps of 1e-3 in ξ. Furthermore, S is set to either the Blasius or the uniform suction values determined above depending on the case being analysed. This results in Figure 4.2.

It is very clear that the use of a constant shear-parameter, S, is not appropriate to describe the boundary layer development. The Blasius solution-derived S results in a large underestimation of the maximum θ^* and predicts a much quicker development towards the far-field (large ξ) solution than reality. However, it predicts more accurately the behaviour close to the Leading Edge (as expected). On the other hand, the uniform suction-derived S parameter results in longer, but still too rapid, development of the boundary layer towards the large

ξ value. Furthermore, it produces the right value of the maximum θ^* (as expected), but describes poorly the behaviour close to the Leading Edge, resulting in an overestimate of the (scaled) boundary layer momentum thickness.

This shows that the variation of S through the boundary layer development is too large to assume the parameter to be constant. The assumption of one value or the other, yields very different BL developments on the flat plate, resulting in a more precise approximate of different parts of the BL. It is clear that a constant S parameter will not yield a satisfactory estimate of the boundary layer development, a better estimate might be obtained by considering a variation of the parameter, as seen in the following section.

4.3 Introduction of a Shape Parameter

A shape parameter, λ, can be introduced such that $S \approx S(\lambda)$. This is similar to Thwaites' method, however, the latter does not include the effects of suction. A similar method is then derived. Defining λ as,

$$\lambda = -\frac{\theta^2}{u_e}\frac{\partial^2 u}{\partial y^2}|_w \tag{4.10}$$

The x-momentum differential equation of the Boundary Layer equations, as given on slide 3a-10, is evaluated at the wall. Note that at the wall: $y = 0$, $u = 0$, $v = v_w$. Furthermore, the steady-state solution is considered $\frac{\partial u}{\partial t} = 0$, and that $\tau_w = \mu\frac{\partial u}{\partial y}|_w$

$$\begin{aligned}
\rho\left(\frac{\partial u}{\partial t} + u\frac{\partial u}{\partial x} + v\frac{\partial u}{\partial y}\right)|_w &= -\frac{\partial p}{\partial x}|_w + \mu\frac{\partial^2 u}{\partial y^2}|_w \\
\Leftrightarrow \rho v_w\frac{\partial u}{\partial y}|_w &= -\frac{\partial p}{\partial x}|_w + \mu\frac{\partial^2 u}{\partial y^2}|_w \\
\Leftrightarrow \rho v_w\frac{\partial u}{\partial y}|_w &= -\frac{\partial p}{\partial x}|_w + \frac{-\mu\lambda u_e}{\theta^2} \\
\Leftrightarrow \lambda &= \frac{-\theta^2}{u_e\mu}\frac{\partial p}{\partial x}|_w - \frac{v_w\theta^2}{\nu u_e}\frac{\partial u}{\partial y}|_w \\
\Leftrightarrow \lambda &= \frac{-\theta^2}{u_e\mu}\frac{\partial p}{\partial x}|_w - \frac{v_w\theta^2}{\nu u_e\mu}\tau_w
\end{aligned}$$

This shows the dependence of the shape factor on both the pressure gradient and the suction velocity. Knowing that $\frac{\partial p}{\partial y} \approx 0$ in the Boundary Layer equations (meaning that $\frac{\partial p}{\partial x}|_w = \frac{\partial p}{\partial x}$), one can evaluate the pressure gradient in the external flow through the x-momentum equation with $\frac{\partial}{\partial t} = 0; u = u_e; v = 0$; and $\frac{\partial^2 u}{\partial y^2} = 0$ (boundary layer-like velocity profile),

$$\begin{aligned}
\rho\left(\frac{\partial u}{\partial t} + u\frac{\partial u}{\partial x} + v\frac{\partial u}{\partial y}\right)|_{y\to\infty} &= -\frac{\partial p}{\partial x} + \mu\frac{\partial^2 u}{\partial y^2}|_{y\to\infty} \\
\rho u_e\frac{\partial u_e}{\partial x} &= -\frac{\partial p}{\partial x}
\end{aligned}$$

Thwaites result is then obtained by putting $v_w = 0$ and substituting the newly found expression for the pressure gradient in the expression for λ derived above. This gives Equation (4.11), which is the familiar formulation of Thwaites, as given on slide 3b-16.

$$\lambda = \frac{-\theta^2}{u_e\mu}\frac{\partial p}{\partial x}|_w - \frac{0\cdot\theta^2}{\nu u_e\mu}\tau_w = \frac{\theta^2}{u_e\mu}\rho u_e\frac{du_e}{dx} = \frac{\theta^2}{\nu}\frac{du_e}{dx} \tag{4.11}$$

For the given problem, the more general formulation presented above can be simplified knowing that $u_e = U_\infty = cst$. The pressure gradient in x is then zero and only the second term of the expression remains.

With the definition of $S = \frac{\theta \tau_w}{\mu U_\infty}$ and the coordinate scaling given by Equation (4.5), the shape factor can be written as follows,

$$\begin{aligned}\lambda &= -\frac{v_w \theta^2}{\nu u_e \mu}\tau_w \\ &= \frac{(-v_w)\theta}{\nu}\left(\frac{\theta \tau_w}{u_e \mu}\right) \\ &= \theta^* S\end{aligned}$$

Therefore, the shape factor for the Blasius and the uniform suction solutions can be obtained:

- **Blasius**: $S_b = \frac{(0.66411)^2}{2}$. $\theta^* = \frac{-v_w}{\nu}\theta = 0$ as the solution assumes no suction. Therefore, $\lambda_b = 0$.
- **Suction profile**: $\theta^* = \frac{1}{2}$ and $S_s = \frac{1}{2}$ were determined earlier. Therefore, $\lambda_s = \frac{1}{4}$.

As the Blasius and the uniform suction solutions essentially bound the problem being considered here, a linear relation can be assumed between the shear parameter and the shape factor can be assumed based on those two data points. Therefore, $S \approx A + B\lambda$. This yields a system of two equations for two unknowns. Considering the Blasius case ($\lambda_b = 0$),

$$S_b = A + B\lambda_b = A \Rightarrow A = \frac{(0.66411)^2}{2}$$

The B variable is then obtained by considering the uniform suction exact solution,

$$S_s = A + B\lambda_s \Leftrightarrow B = \frac{S_s - A}{\lambda_s} \Rightarrow B \approx 1.11792$$

Another way to formulate the problem is by considering the formulation of λ as $\lambda = \theta^* S$. This gives, $S = A + BS\theta^*$, which can be expressed as Equation (4.12).

$$S = \frac{A}{1 - B\theta^*} \tag{4.12}$$

Based on this model, the numerical integration performed earlier for two constant values of S can be reproduced, with an adaptive value of the shear-parameter S. For this purpose, S is recomputed from the value of θ^* at the start of each integration step. This results in Figure 4.3.

It is clear that the result is much better than what was obtained using the models with constant shear parameter. The shape is overall better reproduced, and both the behaviour at the Leading Edge and at large values of ξ are decently reproduced (compared to the constant S models which resulted in a very good approximation of either of the two, but a much worse one of the other). It is clear that this model is then a better alternative to the other two, but the variation in S likely is not linear in the shape factor. The results in terms of accuracy match the expectations: the model is better than the ones previously developed, but is still not extremely accurate. The latter is still expected due to the simplicity of the method used.

4.4 Python Code - Problem 4.E

```
import numpy as np
import matplotlib.pyplot as plt
import csv

Sb = ((0.66411)**2)/2
Ss = 1/2
A = 0.5 * 0.66411**2
B = (0.5 - A)*4
asymp_val_large = 0.5**2
as1 = lambda xi: asymp_val_large + xi*0
as2 = lambda xi: (0.66411 * np.sqrt(xi))**2

```

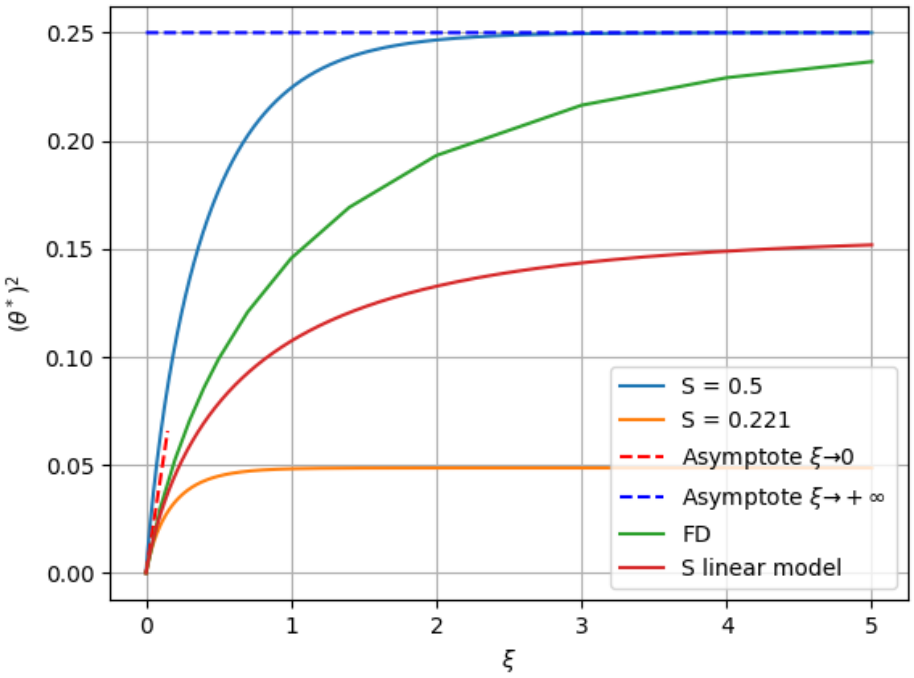

Figure 4.3: The BL development according to Equation (4.6) for different constant S values, and the linear model of S, compared to the Finite Difference solution. The asymptotes of the solution are also given in dashed lines.

```
13 def read_CSV(file):
14     '''
15
16     :param file:
17     :return:
18     '''
19     with open(file, 'r') as file:
20         csvreader = csv.reader(file)
21         csv_headings = next(csvreader)
22         first_line = next(csvreader)
23         first_line = [float(i) for i in first_line]
24         data = np.array(first_line)
25         for row in csvreader:
26             row = [float(i) for i in row]
27             data = np.vstack((data, row))
28     return data
29
30 def dF(th_sqd, S=Sb):
31     return 2 * (S - np.sqrt(th_sqd))  # theta^* is always positive
32
33 def S_lin_model(theta_star):
34     return A/(1-theta_star*B)
35
36 def RK4(y0, S_l, lin_model=False):
37     if lin_model:
38         S_l = Sb
39     dxi = 0.001
40     xi = 0
41     y_list = y0
42     xi_list = [xi]
43     s_list = [S_l]
44
45     y = y0
```

```
    while xi < 5:
        k1 = dF(y, S_l)
        k2 = dF(y + k1 * (dxi / 2), S_l)
        k3 = dF(y + k2 * (dxi / 2), S_l)
        k4 = dF(y + k3 * dxi, S_l)

        y += dxi * (k1 + 2 * k2 + 2 * k3 + k4) / 6
        y_list = np.vstack((y_list, y))
        xi += dxi
        xi_list.append(xi)
        if lin_model:
            S_l = S_lin_model(np.sqrt(y))
        s_list.append(S_l)
    return y_list, xi_list, s_list

theta_sqrd_Sb, xi_list_Sb, s_list_Sb = RK4(0, Sb)
theta_sqrd_Ss, xi_list_Ss, s_list_Ss = RK4(0, Ss)
theta_sqrd_S_lin, xi_list_S_lin, s_list_Slin = RK4(0, Sb, lin_model=True)

num_dat = read_CSV('./data')

as_large = as1(np.array(xi_list_Sb))
as_small = as2(np.array(xi_list_Sb))

plt.figure(1)
plt.plot(xi_list_Ss, theta_sqrd_Ss, label=f'S = {round(Ss, 3)}')
plt.plot(xi_list_Sb, theta_sqrd_Sb, label=f'S = {round(Sb, 3)}')
plt.plot(xi_list_S_lin, theta_sqrd_S_lin, label=f'S linear model')
plt.plot(xi_list_Sb[0:150], as_small[0:150], 'r--', label=r'Asymptote $\xi \to 0$')
plt.plot(xi_list_Sb, as_large, 'b--', label=r'Asymptote $\xi \to +\infty$')
plt.plot(num_dat[:, 0], num_dat[:, 1]**2, label='FD')
plt.legend(loc='lower right')
plt.xlabel(r'$\xi$')
plt.ylabel(r'$(\theta^*)^2 $')
plt.grid(True)
plt.show()
```

Listing 4.1: Problem 4.E Python code

Problem 5.A – Heat Transfer from an Isothermal Flat Plate 5

In this problem, the development of the thermal boundary layer arising due to the heat transfer from a heated wall is considered. In the following, compressibility and viscous effects are neglected. For a flat-plate flow (constant velocity U in the external flow) over an isothermal surface (constant wall temperature T_w), a self-similar thermal boundary layer results, where the shape of the temperature profile still depends on the value of the Prandtl number Pr. In the following, an approximate estimation of the thermal boundary layer development is considered through an integral analysis. The integral momentum and integral heat transfer equations are given by (5.1) and (5.2) respectively.

$$\frac{d}{dx}\int_0^{+\infty} \rho u\,(U-u)\,dy = \mu\frac{\partial u}{\partial y}|_w \qquad (5.1) \qquad \frac{d}{dx}\int_0^{+\infty} u\,(T-T_\infty)\,dy = \frac{-\nu}{Pr}\frac{\partial T}{\partial y}|_w \qquad (5.2)$$

Where use was made of $\tau_w = \mu\frac{\partial u}{\partial y}|_w$, $q_w = -k\frac{\partial T}{\partial y}|_w$, and $Pr = \frac{\mu c_p}{k} = \frac{\nu\rho c_p}{k}$. Those expressions can be used to approximate the boundary layer development, under the assumption of a velocity and temperature profile. In the following, both are assumed to follow linear relations, as given by (5.3) and (5.4).

$$\frac{u}{U} = \begin{cases} \frac{y}{\delta} & \text{if } 0 \le y \le \delta \\ 1 & \text{if } y \ge \delta \end{cases} \qquad (5.3) \qquad \frac{T-T_\infty}{T_w-T_\infty} = \begin{cases} 1-\frac{y}{\delta_T} & \text{if } 0 \le y \le \delta_T \\ 0 & \text{if } y \ge \delta_T \end{cases} \qquad (5.4)$$

Furthermore, for the case $\delta_T \le \delta$, it has been shown during the lectures (see slides 4a-23,24) that,

$$\zeta = \frac{\delta_T}{\delta} = Pr^{\frac{-1}{3}} \qquad (5.5) \qquad s = \frac{q_w/c_p\,(T_w-T_\infty)}{\tau_w/U} = \frac{1}{Pr\zeta} = Pr^{\frac{-2}{3}} \qquad (5.6)$$

where s, is the Reynolds-analogy factor. This case is associated to $Pr \ge 1$. Having laid out the context of the problem, the following sections answer the different questions provided in the assignment.

5.1 ζ and s for $\delta_T \ge \delta$

First, the integral momentum equation is considered to determine an expression for the boundary layer thickness, δ. Based on the velocity velocity profile given by (5.3) (the wall is at $y = 0$),

$$\mu\frac{\partial u}{\partial y}|_w = \tau_w = \mu\frac{\partial(U\frac{y}{\delta})}{\partial y} = \mu\frac{U}{\delta}$$

Therefore, Equation (5.1) can be written as,

$$\begin{aligned} \frac{d}{dx}\int_0^{+\infty} \rho u\,(U-u)\,dy &= \mu\frac{U}{\delta} \\ \Leftrightarrow \rho U^2\frac{d}{dx}\int_0^{+\infty} \frac{u}{U}\left(1-\frac{u}{U}\right)dy &= \mu\frac{U}{\delta} \\ \Leftrightarrow \frac{d\theta}{dx} &= \frac{\nu}{U\delta} \end{aligned} \qquad (5.7)$$

Using the linear velocity profile assumption given by Equation (5.3), the momentum thickness is given by,

$$\theta = \int_0^{+\infty} \frac{u}{U}\left(1-\frac{u}{U}\right)dy$$

$$
\begin{aligned}
&= \int_0^{\delta} \frac{y}{\delta}\left(1-\frac{y}{\delta}\right) dy \\
&= \left[\frac{y^2}{2\delta} - \frac{y^3}{3\delta^2}\right]_0^{\delta} \\
&= \frac{\delta}{2} - \frac{\delta}{3} = \frac{\delta}{6}
\end{aligned} \tag{5.8}
$$

Combining Equations (5.7) and (5.8), the following differential equation is found for δ,

$$\delta \frac{d\delta}{dx} = \frac{6\nu}{U}$$

Which yields,

$$\delta = \sqrt{\frac{12\nu x}{U}} \tag{5.9}$$

Following, the integral heat transfer equation is considered. Note that, as $\delta_T \geq \delta$ in this case, the integral needs to be split in two due to the change in the formulation of the velocity profile at $y = \delta$ shown in Equation (5.3). First considering the right-hand-side (RHS) of Equation (5.2) (based on the temperature profile given by Equation (5.4): $y = 0 : T = T_\infty + (T_w - T_\infty)(1 - \frac{y}{\delta_T})$),

$$RHS = \frac{-\nu}{Pr}\frac{\partial T}{\partial y}|_w = \frac{\nu}{Pr}\frac{(T_w - T_\infty)}{\delta_T}$$

Furthermore, using $\zeta = \frac{\delta_T}{\delta}$,

$$RHS = \frac{\nu}{Pr}\frac{(T_w - T_\infty)}{\zeta\delta} \tag{5.10}$$

The left-hand-side (LHS) is then considered. Using Equation (5.4) $T = T_\infty + (T_w - T_\infty)\left(1 - \frac{1}{\delta_T}\right)$ for $y \leq \delta_T$, and Equation (5.3),

$$
\begin{aligned}
LHS &= \frac{d}{dx}\int_0^{+\infty} u\,(T - T_\infty)\,dy \qquad (5.11)\\
&= U\frac{d}{dx}\int_0^{+\infty} \frac{u}{U}\,(T - T_\infty)\,dy \\
&= U\frac{d}{dx}\left(\int_0^{\delta} \frac{u}{U}\,(T - T_\infty)\,dy + \int_{\delta}^{\delta_T} \frac{u}{U}\,(T - T_\infty)\,dy\right) \\
&= U\frac{d}{dx}\left(\int_0^{\delta} \frac{y}{\delta}\left(T_\infty + (T_w - T_\infty)\left(1 - \frac{y}{\delta_T}\right) - T_\infty\right) dy + \int_{\delta}^{\delta_T} 1 \cdot \left(T_\infty + (T_w - T_\infty)\left(1 - \frac{y}{\delta_T}\right) - T_\infty\right) dy\right) \\
&= U(T_w - T_\infty)\frac{d}{dx}\left(\underbrace{\int_0^{\delta} \frac{y}{\delta}\left(1 - \frac{y}{\delta_T}\right) dy}_{I_1} + \underbrace{\int_{\delta}^{\delta_T} \left(1 - \frac{y}{\delta_T}\right) dy}_{I_2}\right) \qquad (5.12)
\end{aligned}
$$

First solving integral I_1,

$$
\begin{aligned}
I_1 &= \int_0^{\delta} \frac{y}{\delta}\left(1 - \frac{y}{\delta_T}\right) dy \\
&= \int_0^{\delta} \left(\frac{y}{\delta} - \frac{y^2}{\delta\delta_T}\right) dy \\
&= \left[\frac{y^2}{2\delta} - \frac{y^3}{3\delta\delta_T}\right]_0^{\delta}
\end{aligned}
$$

$$= \frac{\delta}{2} - \frac{\delta^2}{3\delta_T}$$

Using $\delta_T = \zeta\delta$,

$$I_1 = \frac{\delta}{2} - \frac{\delta^2}{3\zeta\delta} = \delta\frac{(3\zeta - 2)}{6\zeta} \tag{5.13}$$

Continuing with integral I_2,

$$\begin{aligned} I_2 &= \int_{\delta}^{\delta_T} \left(1 - \frac{y}{\delta_T}\right) dy \\ &= \left[y - \frac{y^2}{2\delta_T}\right]_{\delta}^{\delta_T} \\ &= \left(\delta_T - \frac{\delta_T}{2} - \left(\delta - \frac{\delta^2}{2\delta_T}\right)\right) \\ &= \frac{\delta_T}{2} - \delta + \frac{\delta^2}{2\delta_T} \end{aligned}$$

Using $\delta_T = \zeta\delta$,

$$I_2 = \frac{\zeta\delta}{2} - \frac{2\delta}{2} + \frac{\delta^2}{2\zeta\delta} = \delta\frac{(\zeta^2 - 2\zeta + 1)}{2\zeta} \tag{5.14}$$

Combining Equations (5.11), (5.13) and (5.14) results in,

$$\begin{aligned} LHS &= U(T_w - T_\infty)\frac{d}{dx}\left(I_1 + I_2\right) \\ &= U(T_w - T_\infty)\frac{d}{dx}\left(\delta\frac{(3\zeta - 2)}{6\zeta} + \delta\frac{(\zeta^2 - 2\zeta + 1)}{2\zeta}\right) \\ &= U(T_w - T_\infty)\frac{d}{dx}\left(\delta\frac{(3\zeta^2 - 3\zeta + 1)}{6\zeta}\right) \end{aligned}$$

As ζ is constant for the case of an isothermal plate, Equation (5.2) can be written as,

$$\zeta\frac{(3\zeta^2 - 3\zeta + 1)}{6\zeta}\delta\frac{d\delta}{dx} = \frac{\nu}{PrU}$$

Furthermore, it was shown earlier that $\delta\frac{d\delta}{dx} = \frac{6\nu}{U}$. Which simplifies the expression to Equation (5.15),

$$3\zeta^2 - 3\zeta + 1 = \frac{1}{Pr} \tag{5.15}$$

Given that $\zeta \geq 1$ ($\delta_T \geq \delta$), it can be shown that $Pr \leq 1$. To prove this, the roots of the function $h(\zeta) = Pr - 1$ are determined,

$$\begin{aligned} h(\zeta) = Pr - 1 &= \frac{1}{3\zeta^2 - 3\zeta + 1} - 1 \\ &= \frac{1 - 3\zeta^2 + 3\zeta - 1}{3\zeta^2 - 3\zeta + 1} \\ &= \frac{3\zeta(1 - \zeta)}{3\zeta^2 - 3\zeta + 1} \end{aligned}$$

As the denominator of $h(\zeta)$ has no real roots ($b^2 - 4ac = 9 - 4 \cdot 3 \cdot 1 \leq 0$ in the quadratic formula), the function only changes sign in $\zeta = 0$ and $\zeta = 1$ (from the roots of the numerator). The sign of the function for

$\zeta \geq 1$ is then considered by taking $\zeta = 2$, $h(\zeta = 2) = \frac{-6}{7} \leq 0$. Therefore, $h(\zeta \geq 1) \leq 0$ and $(Pr - 1) \leq 0$. Meaning that $Pr \leq 1$ for $\zeta \geq 1$, which was to be proven.

Having shown that $Pr \leq 1$ for the case considered, an explicit expression for ζ as a function of Pr can be obtained from Equation (5.15),

$$\zeta_{1,2} = \frac{3 \pm \sqrt{9 - 4 \cdot 3\left(1 - \frac{1}{Pr}\right)}}{2 \cdot 3} = \frac{3 \pm \sqrt{\frac{12}{Pr} - 3}}{6}$$

Where it is obvious that for $Pr \leq 1$, the square-root part is always a real number larger than 3. Furthermore, the " $-$ " solution is excluded as it relates to a negative ζ, which is not physical (ratio of two real boundary layer thicknesses is always a positive number). The final expression for ζ is then given by Equation (5.16).

$$\zeta = \frac{\delta_T}{\delta} = \frac{3 + \sqrt{\frac{12}{Pr} - 3}}{6} \tag{5.16}$$

The Reynolds-analogy factor as a function of ζ can then be determined easily from Equation (5.6),

$$s = \frac{q_w / c_p \left(T_w - T_\infty\right)}{\tau_w / U} = \frac{1}{Pr\zeta} = \frac{6}{Pr(3 + \sqrt{12Pr^{-1} - 3})} = \frac{6}{3Pr + \sqrt{12Pr - 3Pr^2}} \tag{5.17}$$

To summarise, for the case $\delta_T \geq \delta$, $Pr \leq 1$, and the expressions for ζ and s are given by,

$$\zeta = \frac{\delta_T}{\delta} = \frac{3 + \sqrt{\frac{12}{Pr} - 3}}{6} \qquad (5.16) \qquad\qquad s = \frac{6}{3Pr + \sqrt{12Pr - 3Pr^2}} \qquad (5.17)$$

5.2 Limit for Pr $\to$ 0

In the limit of Pr goes to zero, the thermal diffusion becomes infinitely larger than the viscous diffusion (as the Prandtl number is the ratio of viscous diffusion to thermal diffusion). Both ζ and s then go to infinity. The behaviour of both expressions is investigated by determining the dominating term from either expressions when $Pr \to 0$. Defining $x = \frac{1}{Pr}$, $Pr \to 0$: $x \to +\infty$ (to facilitate the working outs).

$$\zeta = \frac{\delta_T}{\delta} = \frac{3 + \sqrt{12x - 3}}{6} \qquad\qquad s = \frac{6}{\frac{3}{x} + \sqrt{\frac{12}{x} - \frac{3}{x^2}}}$$

First considering the limit of ζ,

$$\begin{aligned}
\lim_{x \to +\infty} \zeta &= \lim_{x \to +\infty} \left(\frac{1}{2} + \frac{1}{6}\sqrt{12x - 3}\right) \\
&= \lim_{x \to +\infty} \left(\frac{1}{2} + \frac{\sqrt{x}}{6}\sqrt{12 - \frac{3}{x}}\right) \\
&= \lim_{x \to +\infty} \sqrt{x}\left(\frac{1}{2\sqrt{x}} + \frac{1}{6}\sqrt{12 - \frac{3}{x}}\right) \overset{x >> 1}{\approx} \sqrt{x}\left(0 + \frac{1}{6}\sqrt{12 - 0}\right)
\end{aligned}$$

This shows that the overall behaviour of ζ, when $Pr \to 0$, is given by Equation (5.18),

$$\zeta \approx \sqrt{\frac{1}{Pr}}\frac{\sqrt{12}}{6} = \frac{1}{3}\sqrt{\frac{3}{Pr}} = \sqrt{\frac{1}{3Pr}} \tag{5.18}$$

Similarly, the behaviour of the Reynolds-analogy can be investigated,

$$\lim_{x \to +\infty} s = \lim_{x \to +\infty} \frac{6}{\frac{3}{x} + \sqrt{\frac{12}{x} - \frac{3}{x^2}}}$$

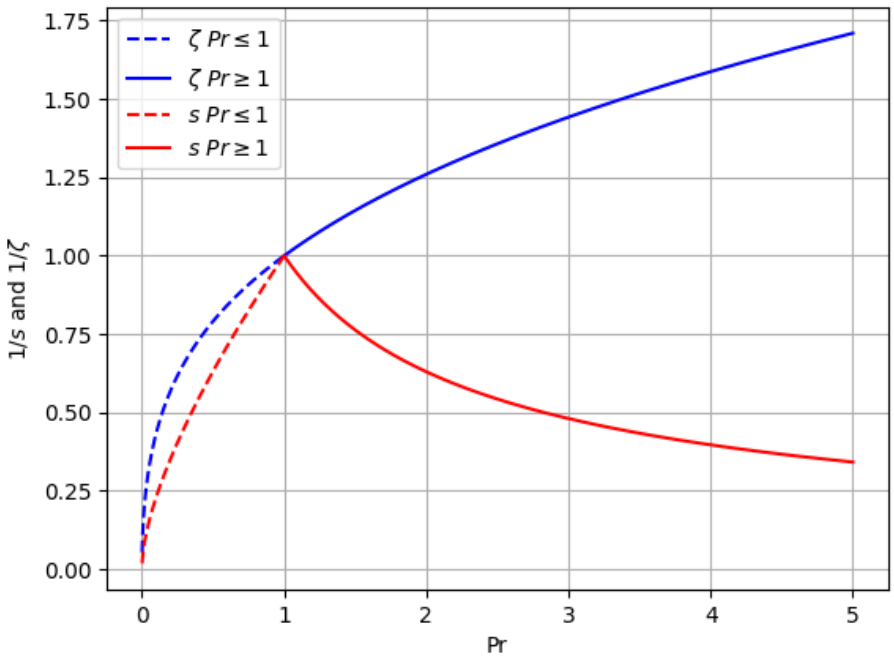

Figure 5.1: Complete approximation for ζ and s on $0 \leq Pr \leq 5$.

$$= \lim_{x \to +\infty} \frac{6}{\frac{1}{\sqrt{x}}\left(\frac{3}{\sqrt{x}} + \sqrt{12 - \frac{3}{x}}\right)} \overset{x>>1}{\approx} \frac{6\sqrt{x}}{0 + \sqrt{12 + 0}}$$

This shows that the overall behaviour of s, when $Pr \to 0$, is given by Equation (5.19),

$$s = \frac{3}{\sqrt{3Pr}} \tag{5.19}$$

This shows that s goes three times faster towards zero than ζ, when $Pr \to 0$. Taking a physical case where $Pr << 1$ (the thermal boundary layer is much larger than the viscous boundary layer thickness, meaning that it is mostly in the inviscid flow), Equations (5.18) and (5.19) can be used to determine both variables with sufficient accuracy.

5.3 Complete Approximation and Match Smoothness

Figure 5.1 shows the complete approximation on the interval $0 \leq Pr \leq 5$. The figure shows that both parts of the approximation match continuously at $Pr = 1$. Although not obvious from the figure (but can be seen by zooming in enough), the first derivatives also seem to match, as demonstrated below.

First considering the continuity at $Pr = 1$, the limits on both sides are considered,

$$\lim_{Pr \to 1^-} \zeta = \lim_{Pr \to 1} \frac{3 + \sqrt{\frac{12}{Pr} - 3}}{6} = \frac{3 + \sqrt{12 - 3}}{6} = 1 \qquad \lim_{Pr \to 1^+} \zeta = \lim_{Pr \to 1} \frac{1}{Pr^{1/3}} = \frac{1}{1} = 1$$

This shows that the complete approximation of ζ is continuous in $Pr = 1$ (and hence over its entire domain). Similarly, for s,

$$\lim_{Pr \to 1^-} s = \lim_{Pr \to 1} \frac{6}{3Pr + \sqrt{12Pr - 3Pr^2}} = \frac{6}{3 + \sqrt{12 - 3}} = 1 \qquad \lim_{Pr \to 1^+} s = \lim_{Pr \to 1} \frac{1}{Pr^{2/3}} = \frac{1}{1} = 1$$

Meaning that s is also continuous at $Pr = 1$. The first order derivatives can also be shown to be continuous at the interface,

$$\lim_{Pr\to 1^-}\frac{\partial\zeta}{\partial Pr}=\lim_{Pr\to 1}\frac{1}{6}\left(\frac{1}{2\sqrt{\frac{12}{Pr}-3}}\right)\frac{-12}{Pr^2}=\frac{1}{12}\frac{-12}{\sqrt{12-3}}=\frac{-1}{3}$$

$$\lim_{Pr\to 1^+}\frac{\partial\zeta}{\partial Pr}=\lim_{Pr\to 1}\frac{-1}{3Pr^{4/3}}=\frac{-1}{3\cdot 1}=\frac{-1}{3}$$

The first derivatives of the expressions for ζ therefore match at the interface $Pr = 1$. Similarly, for the first derivative of s,

$$\lim_{Pr\to 1^-}\frac{\partial s}{\partial Pr}=\lim_{Pr\to 1}\frac{-6\left(3+\frac{(12-6Pr)}{2\sqrt{12Pr-3Pr^2}}\right)}{\left(3Pr+\sqrt{12Pr-3Pr^2}\right)^2}=\frac{-6\left(3+\frac{(12-6)}{2\sqrt{12-3}}\right)}{\left(3+\sqrt{12-3}\right)^2}=\frac{-2}{3}$$

$$\lim_{Pr\to 1^+}\frac{\partial s}{\partial Pr}=\lim_{Pr\to 1}\frac{-2}{3Pr^{5/3}}=\frac{-2}{3\cdot 1}=\frac{-2}{3}$$

This last step confirms that both the expressions of ζ and s on both sides of the interface $Pr = 1$ match smoothly.

5.4 Self-Similar Solution for $Pr << 1$

In the special case for $Pr << 1$, $\delta << \delta_T$, meaning that it can be assumed that the thermal boundary layer takes place completely in the inviscid outer flow. The temperature equation then simplifies to,

$$U\frac{\partial T}{\partial x}=\frac{\nu}{Pr}\frac{\partial^2 T}{\partial y^2} \tag{5.20}$$

5.4.1 Similarity Transformation

Defining,

$$\Theta(\eta)=\frac{T-T_\infty}{T_w-T_\infty} \tag{5.21}$$

$$\eta=\frac{y}{L(x)} \tag{5.22}$$

Where $\Theta(\eta)$ is the self-similar temperature profile with boundary conditions $\Theta(0) = 1$ and $\Theta(+\infty) = 0$. Furthermore, η is the similarity variable with $L(x)$ to be determined (such that the differential equation after the change to the self-similar coordinate system is an ordinary differential equation: only one independent variable being η). First determining the x and y derivatives of η,

$$\frac{\partial\eta}{\partial y}=\frac{1}{L(x)} \qquad \frac{\partial\eta}{\partial x}=\frac{-y}{L(x)^2}\frac{dL(x)}{dx}=\frac{-\eta}{L(x)}\frac{dL}{dx}$$

Following, the different partial derivatives present in Equation (5.20) are determined,

$$\frac{\partial T}{\partial x}=(T_w-T_\infty)\frac{d\Theta}{d\eta}\frac{\partial\eta}{\partial x}=(T_w-T_\infty)\Theta'\frac{-\eta}{L(x)}\frac{dL}{dx}$$

$$\frac{\partial T}{\partial y}=(T_w-T_\infty)\frac{d\Theta}{d\eta}\frac{\partial\eta}{\partial y}=(T_w-T_\infty)\Theta'\frac{1}{L(x)}$$

$$\frac{\partial^2 T}{\partial y^2}=\frac{\partial}{\partial y}\left(\frac{\partial T}{\partial y}\right)=(T_w-T_\infty)\Theta''\frac{1}{L(x)^2}$$

Plugging those expressions in Equation (5.20),

$$\begin{aligned}
&U\frac{\partial T}{\partial x}=\frac{\nu}{Pr}\frac{\partial^2 T}{\partial y^2}\\
&\Leftrightarrow U(T_w-T_\infty)\Theta'\frac{-\eta}{L(x)}\frac{dL}{dx}=\frac{\nu}{Pr}(T_w-T_\infty)\Theta''\frac{1}{L(x)^2}\\
&\Leftrightarrow 0=\Theta''-U\Theta'\frac{(-\eta)}{L}\frac{dL}{dx}\left(\frac{Pr}{\nu}L^2\right)\\
&\Leftrightarrow \Theta''+\left(\frac{UPr}{\nu}L\frac{dL}{dx}\right)\eta\Theta'=0
\end{aligned}$$

The coefficient of the second term needs to be a constant to obtain an ordinary differential equation in η (expected from the similarity transformation). Furthermore, to match the form of the equation given in the assignment, this constant shall be equal to 2:

$$\begin{aligned} \frac{UPr}{\nu} L \frac{dL}{dx} &= 2 \\ \Leftrightarrow LdL &= \frac{2\nu}{UPr} dx \\ \Rightarrow L(x) &= \sqrt{\frac{4\nu x}{UPr}} \end{aligned} \tag{5.23}$$

Therefore, Equation (5.20) can be written as Equation (5.24) with the expression for η given by Equation (5.25).

$$\Theta'' + 2\eta\Theta' = 0 \tag{5.24}$$

$$\eta = \frac{y}{\sqrt{\frac{4\nu x}{UPr}}} \tag{5.25}$$

5.4.2 Solution of the Equation and Nusselt Number

The solution of the equation can be written as Equation (5.26), with $erf(x) = \frac{2}{\sqrt{\pi}} \int_0^x e^{-t^2} dt$. This is in agreement with the boundary conditions mentioned earlier ($\Theta(0) = 1 - \frac{2}{\sqrt{\pi}} \int_0^0 e^{-t^2} dt = 1$ and $\Theta(+\infty) = 1 - \frac{2}{\sqrt{\pi}} \int_0^{+\infty} e^{-t^2} dt = 0$) as $erf(+\infty) = 1$.

$$\Theta(\eta) = (1 - erf(\eta)) \tag{5.26}$$

Furthermore, this gives,

$$\frac{derf(\eta)}{d\eta} = \frac{2}{\sqrt{\pi}} e^{-\eta^2} \qquad \frac{d^2 erf(\eta)}{d\eta^2} = \frac{2}{\sqrt{\pi}} \left(-2\eta e^{-\eta^2}\right)$$

Plugging those derivatives in Equation (5.24) confirms that Equation (5.26) gives indeed the solution to the ordinary differential equation,

$$\frac{2}{\sqrt{\pi}} \left(-2\eta e^{-\eta^2}\right) + 2\eta \frac{2}{\sqrt{\pi}} e^{-\eta^2} = 0$$

The heat transfer at the wall can be computed from the solution, given by Equation (5.27),

$$\begin{aligned} q_w &= -k \frac{\partial T}{\partial y}|_w \\ &= -k(T_w - T_\infty) \frac{d\Theta}{d\eta}|_w \frac{\partial \eta}{\partial y}|_w \\ &= -k(T_w - T_\infty)(-\frac{2}{\sqrt{\pi}} e^0) \frac{1}{L(x)} \\ &= k(T_w - T_\infty) \frac{2}{\sqrt{\pi}} \sqrt{\frac{UPr}{4\nu x}} \end{aligned} \tag{5.27}$$

The local Nusselt number, Nu_x, can then be computed straightforwardly, as given by Equation (5.28),

$$\begin{aligned} Nu_x &= \frac{q_w x}{k(T_w - T_\infty)} \\ &= k(T_w - T_\infty) \frac{2}{\sqrt{\pi}} \sqrt{\frac{UPr}{4\nu x}} \frac{x}{k(T_w - T_\infty)} \\ &= \frac{1}{\sqrt{\pi}} \sqrt{\frac{UxPr}{\nu}} \end{aligned}$$

With the definition of the local Reynolds number $Re_x = \frac{Ux}{\nu}$, this gives,

$$Nu_x = \frac{1}{\sqrt{\pi}}\sqrt{Re_x Pr} \tag{5.28}$$

5.4.3 Reynolds Analogy Factor

The Reynolds analogy factor can be computed for this self-similar boundary layer, with $s = \frac{C_h}{C_f/2}$. The Stanton number C_h is given by,

$$C_h = \frac{Nu_x}{Re_x Pr} = \frac{1}{\sqrt{\pi Re_x Pr}} \tag{5.29}$$

And the friction coefficient is given by (with the wall shear stress from Blasius solution: $\tau_w = 0.332\mu U\sqrt{\frac{U}{x\nu}}$),

$$\frac{C_f}{2} = \frac{\tau_w}{\rho U^2} = \frac{0.332\mu U\sqrt{\frac{U}{x\nu}}}{\rho U^2} = 0.332\sqrt{\frac{\nu}{xU}} = 0.332\sqrt{Re_x^{-1}} \tag{5.30}$$

Combining Equations (5.29) and (5.30) gives the Reynolds analogy factor provided by Equation (5.31)

$$s = \frac{C_h}{\frac{C_f}{2}} = \frac{1}{\sqrt{\pi Re_x Pr}}\frac{\sqrt{Re_x}}{0.332} = \frac{1}{0.332\sqrt{\pi Pr}} \tag{5.31}$$

The coefficient of $\frac{1}{\sqrt{Pr}}$ for the Reynolds analogy factor derived in this section is $a_d = \frac{1}{0.332\sqrt{\pi}} \approx 1.6993$. In comparison, Equation (5.19) shows a coefficient of $a_b = \frac{3}{\sqrt{3}} \approx 1.7321$. This is a difference of only 1.51% between the 'exact' (the former) and the approximate (the latter) approach.

5.5 Python Code - Problem 5.A

```
import numpy as np
import matplotlib.pyplot as plt

i = 1000
Pr1 = np.linspace(0.001, 1, i)
Pr2 = np.linspace(1, 5, 4 * i)

def zeta1(Pr):
    return (3 + np.sqrt((12/Pr) - 3))/6

def zeta2(Pr):
    return Pr**(-1/3)

def s1(Pr):
    return 1/(Pr * zeta1(Pr))

def s2(Pr):
    return 1/(zeta2(Pr) * zeta2(Pr))

Z1_inv = 1/zeta1(Pr1)
Z2_inv = 1/zeta2(Pr2)
S1_inv = 1/s1(Pr1)
S2_inv = 1/s2(Pr2)

plt.figure(1)
plt.plot(Pr1, Z1_inv, 'b--', label=r"$\zeta \ Pr \leq 1$")
plt.plot(Pr2, Z2_inv, 'b', label=r"$\zeta \ Pr \geq 1$")
plt.plot(Pr1, S1_inv, 'r--', label=r"$s \ Pr \leq 1$")
plt.plot(Pr2, S2_inv, 'r', label=r"$s \ Pr \geq 1$")
```

```
30 plt.xlabel('Pr')
31 plt.ylabel(r'$1/s$ and $1/\zeta$')
32 plt.grid(True)
33 plt.legend()
34 plt.savefig('./FigQ5.png')
35 plt.show()
```

Listing 5.1: Problem 5.A Python code

Problem 6.B – Instability and Transition Estimates of Laminar Boundary Layers

6

This problem considers estimates of the location of the point of instability and transition for different flows. The semi-empirical models given by Equations (6.1) and (6.2), derived by Wieghardt and Michel respectively, are considered. The former provides an estimate of the point of instability and the latter an estimate of the point of transition, based on the shape factor $H = \frac{\delta^*}{\theta}$ and a relation between the momentum thickness and Re_x.

$$Re_{\theta,\, crit} = \exp\left(26.3 - 8H\right) \qquad (6.1) \qquad\qquad Re_{\theta,\, trans} = 2.9(Re_{x,trans})^{0.4} \qquad (6.2)$$

Having the context of the problem laid out, the following sections tackle the different questions of the assignment.

6.1 Instability and Transition Estimates

In the following, estimates of the instability and transition points of the flat plate and the stagnation point flows are performed. The boundary layer profiles are characterised by the following:

- **Flat Plate Flow**: $H = 2.591$ and $\theta = 0.664 x Re_x^{\frac{-1}{2}}$.
- **Stagnation Point Flow**: $H = 2.216$ and $\theta = 0.292 x Re_x^{\frac{-1}{2}}$.

Note that both momentum thickness profiles have the same overall formulation: $\theta = xkRe_x^{\frac{-1}{2}}$. This permits to derive more general relations to be applied in each case. First, the relation between Re_θ and Re_x is derived. Noting that $Re_x = \frac{|u_e(x)|x}{\nu}$.

$$Re_\theta = \frac{|u_e(x)|\theta}{\nu} = \frac{|u_e(x)|}{\nu} x k Re_x^{\frac{-1}{2}} = Re_x k Re_x^{\frac{-1}{2}}$$

This yields the relation between Re_θ and Re_x, given by Equation (6.3),

$$Re_\theta = kRe_x^{\frac{1}{2}} \Leftrightarrow Re_x = \left(\frac{Re_\theta}{k}\right)^2 \qquad (6.3)$$

In the cases considered here, this permits to solve Equation (6.2) by replacing $Re_{\theta,trans}$ by its formulation in terms of $Re_{x,\, trans}$. This yields,

$$\begin{aligned} Re_{\theta,\, trans} &= 2.9(Re_{x,\, trans})^{0.4} \\ \Leftrightarrow kRe_{x,\, trans}^{\frac{1}{2}} &= 2.9(Re_{x,\, trans})^{0.4} \\ \Leftrightarrow Re_{x,\, trans}^{0.1} &= \frac{2.9}{k} \end{aligned}$$

This yields Re_x for transition, as estimated by Michel's semi-empirical method, given by Equation (6.4).

$$Re_{x,\, trans} = \left(\frac{2.9}{k}\right)^{10} \qquad (6.4)$$

Table 6.1 provides Re_θ and Re_x for both the instability and transition points. To obtain those values, the following procedure was followed: (1) $Re_{\theta,\, crit}$ was computed based on the shape factor provided above and Equation (6.1); (2) $Re_{x,\, crit}$ is computed from Equation (6.3) and the previous step; (3) $Re_{x,\, trans}$ is obtained from Equation (6.4); (4) $Re_{\theta,\, trans}$ is computed from Equation (6.3) and the previous step.

Table 6.1: Instability and transition points for the flat plate and stagnation point flows.

Flow Type	k	H	$Re_{\theta,\ crit}$	$Re_{x,\ crit}$	$Re_{x,\ trans}$	$Re_{\theta,\ trans}$
Flat Plate	0.664	2.591	≈ 262.96	$\approx 1.568e5$	$\approx 2.5252e6$	$\approx 1.055e3$
Stagnation Point	0.292	2.216	$\approx 5.281e3$	$\approx 3.2717e8$	$\approx 9.3358e9$	$\approx 2.8213e4$

6.2 Effect of the Pressure Gradient

The flat plate flow has a constant external velocity in the boundary layer development direction, this means that the pressure gradient in x is zero for the flat plate case: $\frac{\partial p}{\partial x} = 0$. Furthermore, the stagnation point flow has an external flow velocity $u_e(x) = Bx$, associated with the pressure gradient $\frac{\partial p}{\partial x} = -\rho B^2 x < 0$ (as can be seen from slide 2b-10; this is a favourable pressure gradient). The only difference between those two boundary layer flows being the pressure gradient in the x direction, it is clear from Table 6.1 that a negative pressure gradient has a stabilizing effect on the boundary layer (the instability and transition Re points are much greater for the stagnation flow than the flat plate). This means that the flat plate boundary layer flow will likely (those estimates might be somewhat inaccurate) undergo transition to turbulent flow at a smaller x-location than the stagnation point flow. This is confirmed by slide 5b-10, showing that a negative pressure gradient indeed stabilises the flow.

6.3 Asymptotic Suction Boundary Layer Profile

The velocity profile of the asymptotic suction boundary layer is given by Equation (6.5).

$$\frac{u}{u_e} = 1 - e^{-\eta} \qquad \eta = -\frac{v_w y}{\nu} \tag{6.5}$$

The required suction velocity $-v_w$ to keep the boundary layer at the edge of stability is obtained by determining the BL shape factor, $H = \frac{\delta^*}{\theta}$, and determining Re_θ for a given $-v_w$. The latter is then equated to the $Re_{\theta,\ crit}$ obtained from Equation (6.1). First, the momentum and displacement thicknesses of the boundary layer are computed.

$$\begin{aligned}
\theta &= \int_0^{+\infty} f(y)(1 - f(y))dy \\
&= \int_0^{+\infty} f(\eta)(1 - f(\eta))\frac{\nu}{-v_w}d\eta \\
&= \frac{\nu}{-v_w}\int_0^{+\infty}(1 - e^{-\eta})e^{-\eta}d\eta \\
&= \frac{\nu}{-v_w}\int_0^{+\infty}(e^{-\eta} - e^{-2\eta})d\eta \\
&= \frac{\nu}{-v_w}\lim_{t\to+\infty}\left[-e^{-\eta} + \frac{1}{2}e^{-2\eta}\right]_0^t \\
&= \frac{\nu}{-v_w}(0 + 0 - (-1 + \frac{1}{2})) \\
&= \frac{\nu}{-2v_w}
\end{aligned}$$

Following with the displacement thickness,

$$\begin{aligned}
\delta^* &= \int_0^{+\infty}(1 - f(y))dy \\
&= \int_0^{+\infty}(1 - f(\eta))\frac{\nu}{-v_w}d\eta
\end{aligned}$$

$$
\begin{aligned}
&= \frac{\nu}{-v_w} \int_0^{+\infty} (e^{-\eta}) d\eta \\
&= \frac{\nu}{-v_w} \lim_{t \to +\infty} \left[-e^{-\eta} \right]_0^{+\infty} \\
&= \frac{\nu}{-v_w} (0 - (-1)) = \frac{\nu}{-v_w}
\end{aligned}
$$

Computing the shape factor and Re_θ,

- $H = \frac{\delta^*}{\theta} = 2$.
- $Re_\theta = \frac{|u_e|\theta}{\nu} = \frac{|u_e|}{\nu} \frac{\nu}{-2v_w} = \frac{-|u_e|}{2v_w}$

The point of instability is computed from Equation (6.1) and found to be $Re_{\theta,\, crit} = 2.9732e4$. Equating Re_θ and $Re_{\theta,\, crit}$ results in Equation (6.6).

$$
-v_w = \frac{|u_e|}{2Re_{\theta,\, crit}} \approx 1.6817 \cdot 10^{-5} |u_e| \tag{6.6}
$$

For this value of the suction velocity at the wall, $Re_\theta = Re_{\theta,\, crit}$ throughout the boundary layer, keeping the BL on the margin of stability.

Problem 7.C - Clauser Plot 7

In this problem, the Clauser-plot technique is used to estimate the wall shear stress in a turbulent boundary layer, based on the mean velocity profile (with $\nu = 15 \cdot 10^{-6}$ m^2/s and $U_e = 9.804$ m/s). The technique consists of fitting the second version of the law of the wall to the measured velocity profile. From the original law of the wall,

$$\frac{\bar{u}}{v^*} \approx \frac{1}{\kappa} \ln\left(\frac{yv^*}{\nu}\right) + B \Rightarrow \frac{\bar{u}}{u_e} \approx \frac{v^*}{u_e}\left(\frac{1}{\kappa} \ln\left(\frac{yu_e}{\nu}\frac{v^*}{u_e}\right) + B\right) \tag{7.1}$$

Using $Re_y = \frac{yu_e}{\nu}$ and $\frac{v^*}{u_e} = \sqrt{\frac{C_f}{2}}$ (the latter from slide 6b-22), Equation (7.2) is obtained.

$$\frac{\bar{u}}{u_e} \approx \sqrt{\frac{C_f}{2}}\left(\frac{1}{\kappa} \ln\left(Re_y\sqrt{\frac{C_f}{2}}\right) + B\right) \tag{7.2}$$

7.1 Questions a-b-c: Determination of the Friction Coefficient and Strength of the Wake-Component

The values of κ and B can be considered as near-universal constants with values $\kappa \approx 0.41$ and $B \approx 5$. The only parameter to fit is then the friction coefficient, which was done by using the *curve_fit* function from the SciPy package on Python. It can first be noted that the first three data points can be found to be part of the buffer layer, rather than the overlap layer where the logarithmic law is expected to be valid. This can be seen by computing $y^+ = \frac{yv^*}{\nu} = \frac{yu_e}{\nu}\frac{v^*}{u_e} = Re_y\sqrt{\frac{C_f}{2}}$ once the friction coefficient has been determined (as will be shown below). The first three points are then found to be associated to $y_1^+ \approx 6.41$, $y_2^+ \approx 12.83$, and $y_3^+ \approx 25.65$ respectively, whereas the buffer layer is defined as the points where $5 \leq y^+ \leq 30$ (according to slide 6b-12). Those first three points are then discarded from the final fit displayed below. Furthermore, the best fit for the logarithmic section of the profile was obtained by including only the data points until (and including) y = 18 mm; found by trial and error to determine when the logarithmic nature of the profile breaks down. The velocity profile data points and the fitted law of the wall curve are given in Figure 7.1.

The curve fit is obtained for $C_f \approx 0.003055$ and the strength of the wake, which is defined as the largest difference between the fitted curve and the experimental data, is found to be 1.267 m/s at $Re_y = 30065.6$ (at $y^+ \approx 1175$). For the latter, however, only the data points after the logarithmic region were considered: based on the definition of the wake component provided on slide 6b-17, the wake component occurs at large values of y^+ and not close to the wall.

Figure 7.1: Clauser plot of the provided velocity profile data points and fitted law of the law curve. The orange data points were excluded from the fitting process of the law.

7.2 Python Code - Problem 7.C

```
import numpy as np
import matplotlib.pyplot as plt
import csv
from scipy.optimize import curve_fit

def read_CSV(file):
    '''

    :param file:
    :return:
    '''
    with open(file, 'r') as file:
        csvreader = csv.reader(file)
        csv_headings = next(csvreader)
        first_line = next(csvreader)
        first_line = [float(i) for i in first_line]
        data = np.array(first_line)
        for row in csvreader:
            row = [float(i) for i in row]
            data = np.vstack((data, row))
    return data

# (nearly) Universal constants
kapa = 0.41
B = 5
```

```
26
27 # Air properties
28 nu = 15 * 10**(-6)  # m^2 / s
29 ue = 9.804  # m/s
30
31 # Law of the wall
32 def law_of_the_wall(Rey, r):
33     return r * ((np.log(Rey * r)/kapa) + B)
34
35
36 dat = read_CSV('./Data')
37
38 y = dat[0:, 1]/1000
39 U_ue = dat[0:, 2]
40 Rey = (y * ue)/nu
41
42 i = 20
43 popt, pcov = curve_fit(law_of_the_wall, Rey[3:i], U_ue[3:i])
44 Cf = 2 * popt[0]**2
45 U_ue_law = law_of_the_wall(Rey, *popt)
46 RMS = np.linalg.norm(U_ue[3:i] - U_ue_law[3:i])
47 print(RMS)
48
49 plt.figure(1)
50 plt.scatter(Rey[3:i], U_ue[3:i], label='Experiment - used points')
51 plt.scatter(np.append(Rey[:3], Rey[i:]), np.append(U_ue[:3], U_ue[i:]), label='Experiment
       - unused points')
52 plt.semilogx(Rey, U_ue_law, 'r', label=f'fit: Cf={round(Cf, 6)}')
53 plt.xlabel(r'$Re_{y}$')
54 plt.ylabel(r'$\frac{U}{U_e}$')
55 plt.grid(True)
56 plt.title('Clauser Plot')
57 plt.legend()
58 plt.savefig(f'./Clauser_FINAL.png')
59 plt.show()
60 print(f'Friction coefficient: {Cf}')
61
62 diff = abs(U_ue - U_ue_law)[1:]
63 strength = max(diff)  # *ue
64 ind_strength = np.argmax(diff)
65 print(f'Strength of wake component: {strength*ue} at {Rey[ind_strength+1]}, y_plus = {Rey
      [ind_strength+1] * np.sqrt(Cf/2)}')
66
67 # The first data point is in the viscous sublayer: y+ < 5 and should be discarded
68 y_plus = Rey * np.sqrt(Cf/2)
69 print(y_plus)
```

Listing 7.1: Problem 8.A Python code

Problem 8.A – Turbulence Scaling in the Wall Region – Damping Functions 8

This problem considers the wall region of a 2D incompressible turbulent boundary layer flow. Such flow displays a universal structure, known as the law of the wall, expressing that the properties of the flow can be described uniquely in terms of the wall scaling (wall units). The law of the wall specifies that the velocity profile satisfies an expression of the type,

$$u^+ = f(y^+) \tag{8.1}$$

with $u^+ = \frac{\bar{u}}{v^*}$, $y^+ = \frac{yv^*}{\nu}$ and $v^* = \sqrt{\tau_w/\rho}$. Furthermore, it is common to assume that the total shear stress is approximately constant throughout the wall region. That is,

$$\tau_{visc} + \tau_{turb} = constant = \tau_w \tag{8.2}$$

Having defined the context of the assignment, the following sections address the different questions asked.

8.1 Dimensional Analysis of Kinematic Turbulence Properties

The specific turbulent shear stress ($\frac{\tau_{turb}}{\rho} = -\bar{u'v'}$), the eddy viscosity ($\nu_t$) and the mixing length (l_{mix}) can be non-dimensionalised through a combination of the wall friction velocity ($v^* \sim$ [m/s]) and the viscosity of the flow ($\nu \sim$ [m^2/s]). The required combination is evaluated based on an elementary dimensional analysis:

1. The specific turbulent shear stress: $\frac{\tau_{turb}}{\rho} = -\bar{u'v'} \sim$ [m^2/s^2]. Therefore, $\frac{\tau_{turb}/\rho}{{v^*}^2} \sim$ [-] is non-dimensional, meaning that ${v^*}^2$ is a proper scaling for the specific turbulent shear stress.
2. The eddy viscosity: $\nu_t \sim$ [m^2/s]. Therefore, $\frac{\nu_t}{\nu} \sim$ [-] is non-dimensional, meaning that ν is a proper scaling for the eddy viscosity.
3. The mixing length: $l_{mix} \sim$ [m] $\sim$ [(m^2 s^{-1}) / (m s^{-1})]. Therefore, $\frac{\nu_t}{\frac{\nu}{v^*}} \sim$ [-] is non-dimensional, meaning that $\frac{\nu}{v^*}$ is a proper scaling for the eddy viscosity.

8.2 Kinematic Turbulence Properties Relation to y^+

In the following, the relations of the different kinematic turbulence properties to the wall scaling, y^+, are given. This is done based on their definitions, provided on slide 6a-19 and 6c-3.

8.2.1 Eddy Viscosity

From slide 6a-19, it holds that $\frac{\tau_w}{\rho} = \nu\frac{\partial\bar{u}}{\partial y} + \nu_t\frac{\partial\bar{u}}{\partial y}$. Using the definition of $v^* = \sqrt{\tau_w/\rho}$ and the definitions of u^+ and y^+,

$$\begin{aligned}
\frac{\tau_w}{\rho} = {v^*}^2 &= (\nu + \nu_t)\frac{\partial\bar{u}}{\partial y} \\
\Leftrightarrow {v^*}^2 &= (\nu + \nu_t)\frac{{v^*}^2}{\nu}\frac{\partial u^+}{\partial y^+} \\
\Leftrightarrow \frac{\nu_t}{\nu} &= \frac{1}{\frac{\partial u^+}{\partial y^+}} - 1
\end{aligned}$$

With $f'(y^+) = \frac{1}{\frac{\partial u^+}{\partial y^+}}$, Equation (8.3) is obtained,

$$\frac{\nu_t}{\nu} = \frac{1}{f'(y^+)} - 1 \tag{8.3}$$

8.2.2 Specific Turbulent Shear Stress

From slide 6c-3, it holds that $\frac{\tau_{turb}}{\rho} = \nu_t \frac{\partial \bar{u}}{\partial y}$ (using the result from Equation (8.3)),

$$\begin{aligned} \frac{\tau_{turb}}{\rho} &= \nu_t \frac{v^{*^2}}{\nu} \frac{\partial u^+}{\partial y^+} \\ \Leftrightarrow \frac{\tau_{turb}/\rho}{v^{*^2}} &= \frac{\nu_t}{\nu} \frac{\partial u^+}{\partial y^+} \\ \Leftrightarrow \frac{\tau_{turb}/\rho}{v^{*^2}} &= \left(\frac{1}{f'(y^+)} - 1 \right) f'(y^+) \end{aligned}$$

This yields Equation (8.4),

$$\frac{\tau_{turb}/\rho}{v^{*^2}} = 1 - f'(y^+) \tag{8.4}$$

8.2.3 Mixing Length

From slide 6c-3, it holds that $\nu_t = l_{mix}^2 |\frac{\partial \bar{u}}{\partial y}|$. Furthermore, the Equation (8.3) is used,

$$\begin{aligned} \nu \frac{\nu_t}{\nu} &= l_{mix}^2 \frac{v^{*^2}}{\nu} |\frac{\partial u^+}{\partial y^+}| \\ \Leftrightarrow \frac{\nu_t}{\nu} &= \frac{v^{*^2}}{\nu^2} l_{mix}^2 |f'(y^+)| \\ \Leftrightarrow \left(\frac{1}{f'(y^+)} - 1 \right) \frac{1}{|f'(y^+)|} &= \frac{v^{*^2}}{\nu^2} l_{mix}^2 \end{aligned}$$

Under the assumption of no reverse flow ($f'(y^+) \geq 0$), this results in Equation (8.5),

$$\frac{l_{mix}}{\nu/v^*} = \sqrt{\frac{1}{f'(y^+)^2} - \frac{1}{f'(y^+)}} \tag{8.5}$$

8.3 Behaviour in the Overlap Region

Considering the limit $y^+ >> 1$, which constitutes the overlap region, the velocity profile is known to be logarithmic: $u^+ \propto \ln y^+$. Therefore, $f'(y^+) \propto \frac{1}{y^+}$. This permits to analyse the behaviour of the kinematic properties of turbulent considered earlier, in the overlap region.

8.3.1 Eddy Viscosity

Plugging $f'(y^+) \propto \frac{1}{y^+}$ in Equation (8.3) yields Equation (8.6) (using the scaling for y mentioned earlier). This shows that ν_t is independent of the viscosity in the overlap region and that it grows the further away from the wall (until the point where the logarithmic velocity profile model does not hold anymore).

$$\nu_t = \nu(y^+ - 1) \approx \nu y^+ = v^* y \tag{8.6}$$

8.3.2 Specific Turbulent Shear Stress

Plugging $f'(y^+) \propto \frac{1}{y^+}$ in Equation (8.4) yields Equation (8.7). This shows that as one considers vertical locations further away from the wall, the viscous shear stress vanishes, such that the turbulent shear stress becomes dominant. In the limit of $y^+ >> 1$, the total shear stress is equal to the turbulent shear stress. Furthermore, this shows that the specific turbulent shear stress is independent of the viscosity in the overlap layer.

$$\tau_{turb}/\rho = v^{*^2}\left(1 - \frac{1}{y^+}\right) \approx v^{*^2} = \tau_w/\rho \tag{8.7}$$

8.3.3 Mixing Length

Plugging $f'(y^+) \propto \frac{1}{y^+}$ in Equation (8.5) yields Equation (8.8) (using the scaling for y mentioned earlier). Note that for $y^+ >> 1$, $(y^+)^2 >> y^+$. The mixing length then increases as the distance from the wall increases. Furthermore, this kinematic property is also independent of the viscosity.

$$l_{mix} = \frac{\nu}{v^*}\sqrt{(y^+)^2 - y^+} \approx \frac{\nu}{v^*}\sqrt{(y^+)^2} = \frac{\nu}{v^*}\frac{v^*}{\nu}y = y \tag{8.8}$$

8.4 Limits of Spalding's Law

An accurate description of the velocity profile in the entire turbulent boundary layer is given by Spalding's law, presented by Equation (8.9).

$$y^+ = u^+ + e^{-\kappa B}\left(e^{\kappa u^+} - 1 - (\kappa u^+) - \frac{(\kappa u^+)^2}{2} - \frac{(\kappa u^+)^3}{6}\right) \tag{8.9}$$

Furthermore, note that the Taylor series of the exponential function is given by Equation (8.10).

$$e^x = \sum_{i=0}^{+\infty}\frac{x^i}{i!} \tag{8.10}$$

Considering this profile in the $y^+ << 1$ limit, it is known that $u^+ << 1$ as well, since $u^+ \leq y^+$. The latter can be seen from Equation (8.9), as $y^+ = u^+ + \beta(u^+)$ where $\beta(u^+) \geq 0$. For small values of u^+ (neglecting fifth order terms as they are much smaller than the lower order ones),

$$e^{\kappa u^+} \approx 1 + \kappa u^+ + \frac{(\kappa u^+)^2}{2} + \frac{(\kappa u^+)^3}{6} + \frac{(\kappa u^+)^4}{24}$$

Plugging the approximation in (8.9) yields the limit of the velocity profile in the viscous layer ($y^+ << 1$).

$$y^+ \approx u^+ + e^{-\kappa B}\left(\frac{(\kappa u^+)^4}{24}\right) \approx u^+ \tag{8.11}$$

The limit for $y^+ >> 1$ is obtained under the assumption that u^+ is also significantly larger than 1, meaning that the exponential of κu^+ cannot be represented accurately enough by the first four terms of its series expansion, which are present in the brackets of Equation (8.9). For large enough values of u^+, those first four terms of the Series expansion are then negligible compared to the higher order terms. In that case,

$$e^{\kappa u^+} - 1 - (\kappa u^+) - \frac{(\kappa u^+)^2}{2} - \frac{(\kappa u^+)^3}{6} \approx e^{\kappa u^+}$$

Additionally, the first term, u^+, becomes negligible with respect to the second (which contains the exponential). Therefore,

$$y^+ \approx u^+ + e^{-\kappa B}e^{\kappa u^+} \approx e^{-\kappa B}e^{\kappa u^+}$$

This yields Equation (8.12),

$$
\begin{aligned}
e^{\kappa u^+} &\approx y^+ e^{\kappa B} \\
\kappa u^+ &\approx \ln y^+ + \kappa B \\
u^+ &\approx \frac{1}{\kappa} \ln y^+ + B
\end{aligned} \tag{8.12}
$$

8.5 Damping Functions

Damping functions are defined as the multiplying function of the fully turbulent value, necessary to obtain the effective value (and are particularly useful close to the wall). The fully turbulent values correspond to the relations derived for the overlap region earlier (in Section 8.3, although those relations need to be scaled by $\frac{1}{\kappa}$ to fit the relation found in Equation (8.12)). That is,

$$effective \quad value = damping\ function \times fully\ turbulent\ value$$

The effective values can be obtained from the velocity profile provided by Equation (8.9) and the relations derived in Section 8.2. All the kinematic turbulence properties have a relation to $f'(y^+) = \frac{\partial u^+}{\partial y^+} = \frac{1}{\frac{\partial y^+}{\partial u^+}}$, which can be obtained from,

$$
\begin{aligned}
\frac{\partial y^+}{\partial u^+} &= 1 + e^{-\kappa B}\left(\kappa e^{\kappa u^+} - \kappa - \kappa(\kappa u^+) - \kappa\frac{(\kappa u^+)^2}{2}\right) \\
&= 1 + \kappa e^{-\kappa B}\left(e^{\kappa u^+} - 1 - (\kappa u^+) - \frac{(\kappa u^+)^2}{2}\right)
\end{aligned}
$$

This yields Equation (8.13),

$$f'(y^+) = \frac{\partial u^+}{\partial y^+} = \frac{1}{\frac{\partial y^+}{\partial u^+}} = \frac{1}{1 + \kappa e^{-\kappa B}\left(e^{\kappa u^+} - 1 - (\kappa u^+) - \frac{(\kappa u^+)^2}{2}\right)} \tag{8.13}$$

Based on Equation (8.13), it is possible to determine the damping functions of the eddy viscosity and the mixing length, as seen below.

8.5.1 Eddy Viscosity

Starting from Equation (8.3), the effective value of the eddy viscosity is given by,

$$\frac{\nu_t}{\nu} = \frac{1}{f'(y^+)} - 1 = \kappa e^{-\kappa B}\left(e^{\kappa u^+} - 1 - (\kappa u^+) - \frac{(\kappa u^+)^2}{2}\right)$$

The damping function is then obtained by dividing this effective value by the solution found for the overlap layer specifically, given by Equation (8.12) and repeating the process used in Equation (8.6) (only the scaling by $\frac{1}{\kappa}$ of the velocity profile is different). The fully turbulent value is then given in terms of y^+ as: $\nu_t = \kappa v^* y = \kappa\nu y^+$. Note that Spalding's law was used in the third step.

$$
\begin{aligned}
\phi_{\nu_t} &= \frac{\nu\kappa}{\kappa\nu y^+} e^{-\kappa B}\left(e^{\kappa u^+} - 1 - (\kappa u^+) - \frac{(\kappa u^+)^2}{2}\right) \\
&= \frac{1}{y^+}\left(u^+ - u^+ + e^{-\kappa B}\left(e^{\kappa u^+} - 1 - (\kappa u^+) - \frac{(\kappa u^+)^2}{2} - \frac{(\kappa u^+)^3}{6} + \frac{(\kappa u^+)^3}{6}\right)\right) \\
&= \frac{1}{y^+}\left(u^+ + e^{-\kappa B}\left(e^{\kappa u^+} - 1 - (\kappa u^+) - \frac{(\kappa u^+)^2}{2} - \frac{(\kappa u^+)^3}{6}\right)\right) + \frac{\kappa}{y^+}\left(e^{-\kappa B}\frac{(\kappa u^+)^3}{6} - u^+\right) \\
&= 1 + \frac{1}{y^+}\left(e^{-\kappa B}\frac{(\kappa u^+)^3}{6} - u^+\right)
\end{aligned}
$$

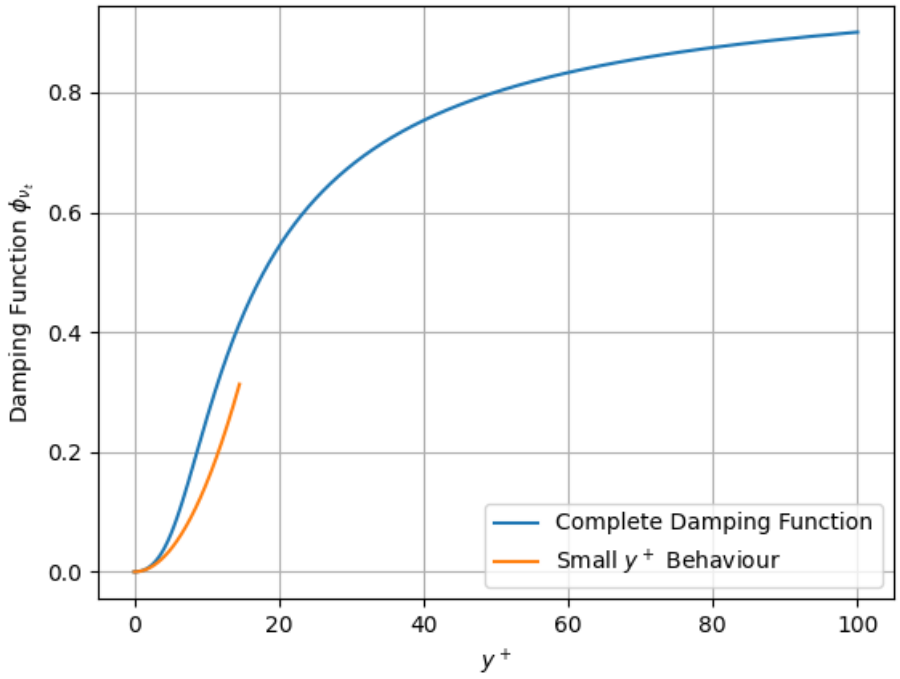

Figure 8.1: Damping function for the eddy viscosity.

The damping function for the eddy viscosity is then given by Equation (8.14),

$$\phi_{\nu_t} = 1 + \frac{1}{y^+}\left(e^{-\kappa B}\frac{(\kappa u^+)^3}{6} - u^+\right) \tag{8.14}$$

The behaviour of the damping function can be considered for small values y^+ by using the limit of Spalding's law for $y^+ << 1$, given by Equation (8.11): $y^+ \approx u^+$. This yields,

$$\phi_{\nu_t, y^+<<1} = \left(e^{-\kappa B}\frac{\kappa(\kappa u^+)^2}{6}\right) \approx \left(e^{-\kappa B}\frac{\kappa(\kappa y^+)^2}{6}\right)$$

which describes a parabola (looking at the region where $y^+ \approx u^+$). This means that the damping function starts from zero and grows quickly with the square of the scaled wall coordinates, when it is still in the viscous layer. However, this predicted behaviour breaks down quickly as it is only valid for small values of y^+ (only the first non-zero term of the Taylor expansion is considered, and an assumption on the behaviour of y^+ is used) and the quadratic behaviour rather quickly stops being representative (see Figure 8.1).

The damping function for the eddy viscosity is plotted in Figure 8.1, as given by Equation (8.14) (the values of u^+ were specified and the associated values of y^+ were computed from Equation (8.9)). It is clear from this figure that the function goes from zero to one, indicating that the eddy viscosity is essentially zero close to the wall (viscous sublayer), meaning that the viscous stresses take over turbulent stresses in that region. Furthermore, further away from the wall, the turbulent viscosity reaches its maximum, fully turbulent, value (derived earlier). This fully turbulent value is reached a bit farther away from the wall than $y^+ = 100$. The behaviour for small y^+ is in accordance with what was determined above.

8.5.2 Mixing Length

Starting from Equation (8.5), and plugging in the expression for $f'(y^+)$,

$$l_{mix} = \frac{\nu}{v^*}\sqrt{\frac{1}{(f'(y^+))^2} - \frac{1}{f'(y^+)}}$$

$$= \frac{\nu}{v^*}\sqrt{\left(1 + \kappa e^{-\kappa B}\left(e^{\kappa u^+} - 1 - (\kappa u^+) - \frac{(\kappa u^+)^2}{2}\right)\right)^2 - \left(1 + \kappa e^{-\kappa B}\left(e^{\kappa u^+} - 1 - (\kappa u^+) - \frac{(\kappa u^+)^2}{2}\right)\right)}$$

$$= \frac{\nu}{v^*}\left(1+\kappa e^{-\kappa B}\left(e^{\kappa u^+}-1-(\kappa u^+)-\frac{(\kappa u^+)^2}{2}\right)\right)\sqrt{1-\frac{1}{\left(1+\kappa e^{-\kappa B}\left(e^{\kappa u^+}-1-(\kappa u^+)-\frac{(\kappa u^+)^2}{2}\right)\right)}}$$

The damping function is then obtained by dividing the effective value (shown in the previous equation) by the fully turbulent value which is valid in the overlap region. The latter is found by re-iterating the process used in Equation (8.8), with the limit of Spalding's law for large y^+ given in Equation (8.12). This gives, $l_{mix} = \frac{\nu}{v^*}\kappa y^+$. Therefore,

$$\begin{aligned}
\phi_{l_{mix}} &= \frac{\nu}{v^*}\frac{1}{\frac{\nu}{v^*}\kappa y^+}\left(1+\kappa e^{-\kappa B}\left(e^{\kappa u^+}-1-(\kappa u^+)-\frac{(\kappa u^+)^2}{2}\right)\right)\sqrt{1-\frac{1}{\left(1+\kappa e^{-\kappa B}\left(e^{\kappa u^+}-1-(\kappa u^+)-\frac{(\kappa u^+)^2}{2}\right)\right)}} \\
&= \frac{1}{\kappa y^+}\left(1+\kappa e^{-\kappa B}\left(e^{\kappa u^+}-1-(\kappa u^+)-\frac{(\kappa u^+)^2}{2}\right)\right)\sqrt{1-\frac{1}{\left(1+\kappa e^{-\kappa B}\left(e^{\kappa u^+}-1-(\kappa u^+)-\frac{(\kappa u^+)^2}{2}\right)\right)}} \\
&= \frac{1}{\kappa y^+}\left(1+(\kappa u^+-\kappa u^+)+\kappa e^{-\kappa B}\left(e^{\kappa u^+}-1-(\kappa u^+)-\frac{(\kappa u^+)^2}{2}-\left(\frac{(\kappa u^+)^3}{6}-\frac{(\kappa u^+)^3}{6}\right)\right)\right) \\
&\sqrt{1-\frac{1}{\left(1+(\kappa u^+-\kappa u^+)+\kappa e^{-\kappa B}\left(e^{\kappa u^+}-1-(\kappa u^+)-\frac{(\kappa u^+)^2}{2}-\left(\frac{(\kappa u^+)^3}{6}-\frac{(\kappa u^+)^3}{6}\right)\right)\right)}} \\
&= \frac{1}{\kappa y^+}\left(1-\kappa u^+ +\kappa e^{-\kappa B}\frac{(\kappa u^+)^3}{6}+\kappa y^+\right)\sqrt{1-\frac{1}{\left(1-\kappa u^+ +\kappa e^{-\kappa B}\frac{(\kappa u^+)^3}{6}+\kappa y^+\right)}} \\
&= \frac{1}{\kappa y^+}\sqrt{\left(1-\kappa u^+ +\kappa e^{-\kappa B}\frac{(\kappa u^+)^3}{6}+\kappa y^+\right)^2-\left(1-\kappa u^+ +\kappa e^{-\kappa B}\frac{(\kappa u^+)^3}{6}+\kappa y^+\right)} \\
&= \frac{1}{\kappa y^+}\sqrt{\left(1-\kappa u^+ +\kappa e^{-\kappa B}\frac{(\kappa u^+)^3}{6}+\kappa y^+\right)\left(1-\kappa u^+ +\kappa e^{-\kappa B}\frac{(\kappa u^+)^3}{6}+\kappa y^+-1\right)}
\end{aligned}$$

The damping function for the mixing length is then given by Equation (8.15),

$$\phi_{l_{mix}} = \frac{1}{\kappa y^+}\sqrt{\left(1-\kappa u^+ +\kappa e^{-\kappa B}\frac{(\kappa u^+)^3}{6}+\kappa y^+\right)\left(\kappa y^+ -\kappa u^+ +\kappa e^{-\kappa B}\frac{(\kappa u^+)^3}{6}\right)} \tag{8.15}$$

To find the value of the damping function for $y^+ << 1$, similarly to the analysis of the behaviour of the eddy viscosity damping function for small y^+, the limit of Spalding's law for small y^+ was used: $y^+ \approx u^+$, this yields,

$$\phi_{l_{mix},y^+<<1} = \frac{1}{\kappa y^+}\sqrt{\left(1+\kappa e^{-\kappa B}\frac{(\kappa u^+)^3}{6}\right)\left(\kappa e^{-\kappa B}\frac{(\kappa u^+)^3}{6}\right)}$$

Furthermore, $\kappa e^{-\kappa B}\frac{(\kappa u^+)^3}{6} << 1$, yielding,

$$\begin{aligned}
\phi_{l_{mix},y^+<<1} &= \frac{1}{\kappa y^+}\sqrt{\left(\kappa e^{-\kappa B}\frac{(\kappa u^+)^3}{6}\right)} \\
&= \sqrt{\left(\kappa e^{-\kappa B}\frac{(\kappa y^+)^3}{6(\kappa y^+)^2}\right)} \\
\phi_{l_{mix},y^+<<1} &= \kappa\sqrt{e^{-\kappa B}\frac{y^+}{6}}
\end{aligned}$$

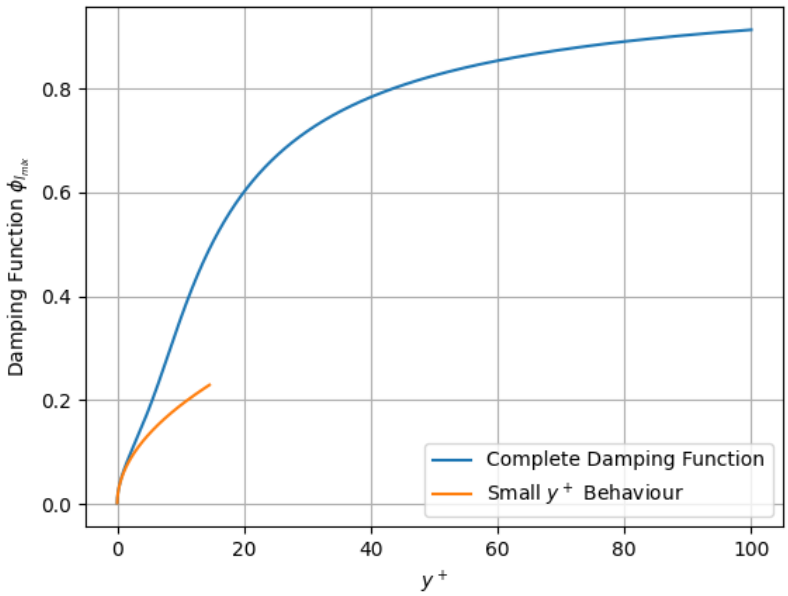

Figure 8.2: Damping function for the mixing length.

(8.16)

which describes a square-root in y^+. The square-root like behaviour shows that the damping function first grows quickly (infinite derivative at the wall), however, the validity of the relation breaks down before the more slowly-growing characteristic square-root behaviour at larger values of y^+ can be seen. Furthermore, the estimate for small y^+ gives a good match with the complete damping function close to the wall but quickly breaks down as it is only valid for small values of y^+.

The damping function for the mixing length is plotted in Figure 8.2, as given by Equation (8.15) (the values of u^+ were specified and the associated values of y^+ were computed from Equation (8.9)). Similarly to the eddy viscosity discussed above, it is clear from this figure that the function goes from zero to one, indicating that the mixing length is essentially zero close to the wall (viscous sublayer). Furthermore, further away from the wall, the mixing length reaches its maximum, fully turbulent, value (derived earlier). This fully turbulent value is reached a bit farther away from the wall than $y^+ = 100$. Furthermore, it is also clear that the behaviour of the function for small values of y^+ is significantly different from the damping function of the eddy viscosity ($\phi_{l_{mix}}$ is more vertical from the start), resulting in an overall faster growth of the mixing length (reaching 80% of the full value close to $y^+ = 45$ while the eddy viscosity reached that percentage at around $y^+ = 50$).

8.6 Python Code - Problem 8.A

```
import numpy as np
import matplotlib.pyplot as plt


k = 0.41
B = 5
nu = 15 * 10**(-6)
y_plus = lambda u: u + np.e**(-k * B) * (np.e**(k * u) - 1 - k* u - 0.5 * (k*u)**2 - ((k*
    u)**3)/6)
nu_t_to_nu = lambda u: k * np.e**(- k * B) * (np.e**(k*u) - 1 - (k*u)- 0.5 * (k*u)**2)
l_mix_adim = lambda u: np.sqrt((1+k*np.e**(-k * B) * (np.e**(k*u) - 1 - (k*u) - 0.5 * (k*
    u)**2))**2 - (1+k*np.e**(-k * B) * (np.e**(k*u) - 1 - (k*u) - 0.5 * (k*u)**2)))

def phi_vt(u_s, y_s):
    return 1 + (1/(y_s)) * (np.e**(-k * B) * ((k * u_s)**3)/6 - u_s)
```

```
14
15 def phi_lmix(u_s, y_s):
16     return ((((1/k) - u_s + np.e**(-k * B) * (1/6) * (k * u_s)**3)/y_s) + 1) * np.sqrt(1
       - 1/(1 - k * u_s + k * np.e**(-k * B) * (1/6) * (k * u_s)**3 + k * y_s))
17
18 u = np.arange(0.001, 50, 0.001)
19 y = y_plus(u)
20 u_under_y_100 = u[y<=100]
21 y_under_100 = y[y<=100]
22
23 vt_damp_under_y_100 = phi_vt(u_under_y_100, y_under_100)
24 lmix_damp_under_y_100 = phi_lmix(u_under_y_100, y_under_100)
25
26 plt.figure(1)
27 plt.plot(y_under_100, vt_damp_under_y_100, label='Complete Damping Function')
28 #plt.plot(y_under_100, nu_t_to_nu(u_under_y_100))
29 plt.plot(y_under_100[:10000], k*(np.e**(-k*B)*(k*y_under_100[:10000])**2)/6, label=r'
       Small $y^+$ Behaviour')
30 plt.grid(True)
31 plt.xlabel(r'$y^+$')
32 plt.ylabel(r'Damping Function $\phi_{\nu_{t}}$')
33 plt.legend()
34 #plt.savefig('./eddy.png')
35
36 plt.figure(2)
37 plt.plot(y_under_100, lmix_damp_under_y_100, label='Complete Damping Function')
38 plt.plot(y_under_100[:10000], k*np.sqrt(np.e**(-k*B) * y_under_100[:10000]/6), label=r'
       Small $y^+$ Behaviour')
39 #plt.plot(y_under_100, l_mix_adim(u_under_y_100))
40 plt.grid(True)
41 plt.xlabel(r'$y^+$')
42 plt.ylabel(r'Damping Function $\phi_{l_{mix}}$')
43 plt.legend()
44 plt.savefig('./lmix.png')
45 plt.show()
```

Listing 8.1: Problem 8.A Python code